Atomic and molecular adsorption on Ni(111)

Yunhai Bai , Demetrios Kirvassilis , Lang Xu , Manos Mavrikakis

PII: S0039-6028(18)30496-5
DOI: https://doi.org/10.1016/j.susc.2018.08.004
Reference: SUSC 21304

To appear in: *Surface Science*

Received date: 11 June 2018
Revised date: 5 August 2018
Accepted date: 7 August 2018

Please cite this article as: Yunhai Bai , Demetrios Kirvassilis , Lang Xu , Manos Mavrikakis , Atomic and molecular adsorption on Ni(111), *Surface Science* (2018), doi: https://doi.org/10.1016/j.susc.2018.08.004

Highlights

- Calculated binding structures and energies of atoms, molecules, and molecular fragments on Ni(111)
- Calculated vibrational frequencies of adsorbates on Ni(111)
- Estimated diffusion paths and barriers for adsorbates on Ni(111)
- Evaluated thermochemistry for the decomposition of NO, CO, NH_3, N_2, and CH_4 on Ni(111)

Atomic and molecular adsorption on Ni(111)

Yunhai Bai, Demetrios Kirvassilis, Lang Xu, Manos Mavrikakis*

Department of Chemical & Biological Engineering, University of Wisconsin-Madison, Madison, WI 53706

*Corresponding author: emavrikakis@wisc.edu

Abstract

Periodic, self-consistent density functional theory (DFT-GGA) calculations are used to study the adsorption properties of atomic species (H, C, N, O, and S), molecular species (CO, HCN, NH_3, N_2, and NO), and molecular fragments (CH, CH_2, CH_3, CN, NH, NH_2, HCO, COH, HNO, NOH, and OH) on Ni(111), at a 1/4 monolayer coverage. For each of these species, we calculate the binding energies at all possible sites and determine the optimal binding configuration, calculate the vibrational frequencies and deformation energy at the preferred adsorption site, and estimate the diffusion barrier on Ni(111). Good agreement is found when comparing our calculated results with available literature values determined using various experimental or theoretical methods. Based on the calculated binding energies, thermochemistry potential energy surfaces for adsorption and decomposition of NO, CO, NH_3, N_2, and CH_4 are developed, showing that the decomposition of all these molecular species is energetically more favorable than their desorption from Ni(111).

Keywords: density functional theory; nickel; adsorption; catalysis; diffusion.

1 Introduction

Nickel is an important catalyst that has many industrial applications. In particular, nickel has been widely used in the reforming (including both steam reforming and CO_2 reforming) processes to produce syngas [1-7]. It has also been used as a hydrogenation and hydrogenolysis catalyst in many chemical reactions [8-14]. Nickel-based catalysts have shown high activity in the cross-coupling reactions, the Heck reactions, and the reductive coupling reactions [15,16]. In addition, Ni is an important component in solid oxide fuel cell (SOFC) anodes, in biomass gasification catalysts, and in petroleum hydro-treating catalysts (e.g., hydro-denitrogenation to reduce NO_x and hydro-desulphurization to reduce SO_x) [17-25]. Due to the broad application of nickel in catalytic reactions, the interactions of atomic and molecular species with Ni(111), the most stable crystallographic structure of nickel, have been extensively studied with various techniques.

Nickel is an excellent hydrogenation catalyst, and thus hydrogen adsorption on nickel has been the subject of many surface science studies, e.g., low energy electron diffraction (LEED) [26-29], Auger electron spectroscopy (AES) [26], electron energy loss spectroscopy (EELS) [26, 29], flash desorption [26], work function measurements [26-27], thermal desorption spectroscopy (TDS) [27], temperature programmed desorption (TPD) [30], high-resolution electron energy loss spectroscopy (HREELS) [31,32], scanning tunneling microscopy (STM) [33], and density functional theory (DFT) [34-36]. In addition to surface hydrogen, subsurface hydrogen embedded in Ni, which has been found to have unique reactivity, and its role in hydrogenation reactions, have also been examined both experimentally and theoretically [34-44].

In addition to H, other atomic species, including C, N, O, and S, have also been characterized extensively on Ni(111). Carbon intermediates are present on Ni-based catalysts in reforming

processes [5, 45] and in the methanation reaction [10, 46]. The interaction of carbon with Ni surfaces has been studied using a variety of experimental techniques, including LEED [47-50], AES [47, 48, 51], STM [48, 51], and theoretical calculations [6, 52-54]. The adsorption of atomic oxygen on Ni(111) has been studied with LEED [47, 55-59], AES [47, 55], near-edge X-ray absorption fine structure (NEXAFS) [60], electron energy loss fine structures spectroscopy (EELFSS) [61,62], high-energy He ion scattering (HEIS) [62,63], single-crystal adsorption calorimeter [64], surface extended X-ray absorption fine structure (SEXAFS) [65], EELS [66], HREELS [67], STM [68], X-ray photoelectron spectroscopy (XPS) [67], and DFT [53, 69, 70]. The adsorption of atomic sulfur on Ni(111) has been examined with STM [51, 71, 72], LEED [47, 57, 71, 73-78], AES [47, 51, 71, 76], XPS [78], soft X-ray photoelectron spectroscopy (SXPS) [79], HREELS [79], SEXAFS [80], normal-incidence X-ray standing wavefield absorption (NIXSW) [76], impact collision ion scattering spectroscopy (ICISS) [81], and DFT [82-84].

Nickel is a widely used catalyst in the methanation reaction and the steam/CO_2 reforming of CH_4. Previous studies have indicated that CH_x are important reaction intermediates and are formed on catalyst surfaces in these processes [85]. Interactions of these species with Ni(111) have been the subject of extensive studies. In particular, EELS [86], HREELS [87-89], thermogravimetric analysis (TGA) [4], extended X-ray absorption spectroscopy (EXAFS) [4], ultraviolet photoelectron spectroscopy (UPS) [90], TPD [90], LEED [90], secondary ion mass spectrometry (SIMS) [85], XPS [85], and theoretical calculations [4, 11, 91-94] have been employed in the study of CH_x species adsorption and the reactions involving those intermediates on nickel surfaces.

CO is one of the products in the reforming process. Therefore, CO adsorption on Ni is of fundamental importance and is one of the most thoroughly studied adsorption systems. CO adsorption process, adsorption structure, and diffusion on Ni(111) have been studied by LEED [95-102], AES [95, 97-98], SEXAFS [103], energy-scan photoelectron diffraction (EPD) [103], UPS [97], TDS [98], HREELS [104, 105], infrared reflection absorption spectroscopy (IRAS) [99, 106, 107], TPD [99, 106, 107], Fourier transform reflection absorption infrared spectroscopy (FT-RAIRS) [108], XPS [109], and theoretical calculations [53, 110, 111].

Nickel has been identified as a very promising catalyst for the ammonia decomposition reaction, which starts with the dehydrogenation of NH_3 to form NH_2, NH and N species, followed by the recombination of N atoms to form N_2 and of H atoms to form H_2 [112-113]. The interactions between intermediates in NH_3 decomposition and Ni(111) have been extensively studied. In particular, N_2 adsorption on nickel has been studied with infrared spectroscopy (IR) [114], electron microscopy (EM) [114], LEED [115, 116], electron spectroscopy [117], reflection absorption infrared spectroscopy (RAIRS) [115], Fourier transform infrared reflection absorption spectroscopy (FT-IRAS) [116], XPS [118, 119], UPS [118, 119], metastable impact electron spectroscopy (MIES) [120], TPD [119], and DFT [4]. The interactions between NH_x and Ni(111) have been characterized with LEED [121-124], AES [121], HREELS [121, 125], TDS [123, 124, 126], angle-resolved photoemission [123], temperature-programmed reaction spectroscopy (TPRS) [121], UPS [122], TPD [122, 127], electron stimulated desorption ion angular distribution (ESDIAD) [122, 124, 127], photoelectron diffraction (PhD) [128], FT-IRAS [129], surface Penning ionization spectroscopy (SPIES) [126], and theoretical calculations [112, 130-134].

It is well established that NO adsorbs molecularly on Ni at low temperatures [135-143]. NO adsorption on Ni(111) is a widely studied research topic and a number of techniques have been employed in these studies, including LEED [135, 136, 138, 140, 142, 144-150], AES [138, 140-142, 144], UPS [135, 138, 149], flash desorption spectroscopy [138], FT-RAIR [141, 142, 144], TDS [142], XPS [135, 148], SXPS [145], X-ray excited Auger spectroscopy (XAES) [135], metastable quenching electron spectroscopy (MQS) [139], FTIR [137, 140, 143], EELS [143], HREELS [140], ESDIAD [136], PhD [145], SEXAFS [151], NEXAFS [150], and DFT [152].

In this work, we present a systematic study of adsorption structures, binding energies, vibrational frequencies, deformation energies, and diffusion barriers for the adsorption of atomic species (H, C, N, O, and S), molecular species (CO, HCN, NH_3, N_2, and NO), and molecular fragments (CH, CH_2, CH_3, CN, NH, NH_2, HCO, COH, HNO, NOH, and OH) on Ni(111), using periodic, self-consistent density functional theory (DFT-GGA) calculations. This study is similar to our previously published database papers, in which the adsorption properties of these adsorbates on Rh(111) [153], Ir(111) [154], Pt(111) [155], Pd(111) [156], Ru(0001) [157], Re(0001) [158], Au(111) [159], Fe(110) [160], Ag(111) [161] and Cu(111) [162] are analyzed. Same computational methods are used in our work all along, so that one can directly compare adsorption properties of surface species on various transition metal single crystal surfaces across the periodic table. Our calculated values are compared with available experimental values, and can be added to other electronically accessible databases [163].

2 Computational Methods

All calculations are performed using the DACAPO total energy code [164, 165] based on spin-polarized DFT. The Ni(111) surface is modeled by a four-layer slab with a 2 × 2 unit cell,

corresponding to a surface coverage of 1/4 monolayer (ML) for a single adsorbate per unit cell. The unit cell is periodically repeated in a super cell geometry, and successive slabs are separated by five equivalent layers of vacuum. The top two layers of the slab are allowed to relax. Adsorption is allowed on only one of the two exposed surfaces, and the electrostatic potential is adjusted accordingly [166, 167]. The surface Brillouin zone is sampled at 18 special Chadi-Cohen k-points [168]. Ultrasoft Vanderbilt pseudopotentials [169] are utilized to describe ionic cores, and the Kohn-Sham one-electron valence states are expanded on the basis of plane waves with kinetic energy below 25 Ry. Self-consistent GGA-PW91 functional is used to describe the exchange-correlation potential and energy [170-171]. The electron density is determined by iterative diagonalization of the Kohn-Sham Hamiltonian, Fermi population of the Kohn-Sham states (k_BT = 0.1 eV), and Pulay mixing of the resulting electronic density [172]. All total energies have been extrapolated to k_BT = 0 eV. Additionally, values calculated non-self-consistently using the RPBE functional are listed [164]. The calculated equilibrium lattice constant for bulk Ni is 3.52 Å, in agreement with the experimental value of 3.52 Å [173]. The calculated magnetic moment per Ni atom is 0.73 μ_B, in comparison with the experimental value of 0.62 μ_B [174]. The calculated gas-phase atomization energies (both self-consistent PW91 and non-self-consistent RPBE) for some of the adsorbate species are listed in Table 1, along with available experimental values at 0 K [175].

Table 1 Calculated and experimental gas-phase atomization energies at 0 K.

Species	Atomization energy (eV)		
	PW91	RPBE	Exp.
CH	3.65	3.64	3.45
CH_2	8.49	8.37	7.81
CH_3	13.39	13.16	12.54
CH_4	18.08	17.74	17.02
CO	10.96	10.59	11.11
NH	3.74	3.38	3.40

NH_2	7.96	7.50	7.36
NH_3	12.74	12.50	12.00
N_2	9.63	9.47	9.76
NO	6.73	6.50	6.51
OH	4.60	4.53	4.41
O_2	5.64	5.20	5.12

The species here are those for which experimental values are available. The experimental values are taken from Reference [175].

Binding energy (B.E.) is defined as B.E. = $E_{total} - E_{clean} - E_{gas}$, where E_{total}, E_{clean} and E_{gas} are the total energies of the Ni(111) slab with adsorbate, the clean Ni(111) slab, and the adsorbate species in the gas phase, respectively. Binding energies calculated using both exchange-correlation functionals are reported, with the RPBE values shown in square brackets. Convergence of binding energies with respect to various calculation parameters is verified. The average magnetic moment per surface Ni atom that binds directly to the adsorbate in each adsorption state is also calculated.

The deformation energy (ΔE), i.e., the change in slab energy upon the adsorption of an adsorbate, is calculated by subtracting the energy of the relaxed, clean Ni(111) slab from the energy of the relaxed slab, frozen after the adsorption of the adsorbate but with the adsorbate removed. Based on this definition, deformation energy is always positive and a larger number indicates a more pronounced effect of the adsorbate's adsorption on the Ni(111) slab.

The vibrational frequencies are calculated using the harmonic oscillator assumption by diagonalization of the mass-weighted Hessian matrix. The second derivatives of energy are evaluated using a finite difference approximation [35]. The diffusion barrier of an adsorbate is estimated by identifying a plausible diffusion path that connects neighboring minima on the potential energy surface (PES) via a metastable site, and then calculating the energy difference between the metastable state and the most stable state on that particular path.

3 Results and Discussion

In the following section, we will present our calculated results for all studied adsorbates on Ni(111) and compare those with experimental results, when available. Results include adsorption site preferences, binding energies and average magnetic moment per surface Ni atom that binds to the adsorbate (Tables 2 and 7), adsorption structures (Table 5 and Figure 2), surface deformation energies (Table 6), estimated diffusion barriers (Table 4), and vibrational frequencies (Tables 3, 8, and 9). At the end of this section, we construct potential energy surfaces (Figure 3) for the NO, CO, NH_3, N_2, and CH_4 decomposition reactions.

Table 2 Binding energies in PW91 [RPBE in brackets], site preferences and average magnetic moment per surface Ni atom (that directly binds to the adsorbate) for atomic species on Ni(111). Reference state is the adsorbate in the gas phase at infinite separation from the slab. For comparison, the magnetic moment per surface Ni atom in the clean relaxed slab is $0.68\mu_B$.

Adsorbate	Preferred Site		Binding energy (eV)			Magnetic moment per surface Ni atom (μ_B)	
	Calc.	Exp.	fcc	hcp	Exp.	fcc	hcp
H	fcc	hollow[a]	**-2.89** **[-2.72]**	-2.88 [-2.71]	-2.73[b], -2.74[c]	0.57	0.56
C	hcp		-6.54 [-6.03]	**-6.56** **[-6.04]**		0.13	0.14
N	fcc		**-5.01** **[-4.53]**	-4.98 [-4.49]		0.11	0.13
O	fcc	fcc[d]	**-5.13** **[-4.52]**	-5.02 [-4.42]	-4.84[e]	0.49	0.50
S	fcc	fcc[f]	**-5.12** **[-4.62]**	-5.07 [-4.57]		0.47	0.49

Numbers in bold indicate the binding energies of atomic species at the most stable site.

[a] LEED [27], EELS [29]

[b] H_2, flash desorption spectroscopy [176] (adjusted using experimental atomization energy from Ref [175])

[c] H_2, flash desorption spectroscopy [26] (adjusted using experimental atomization energy from Ref [175])

[d] NEXAFS [60], LEED [58]

[e] O_2, single-crystal adsorption calorimetry [176] (adjusted using experimental atomization energy from Ref [175])

[f] LEED [75, 77], NIXSW [76], ICISS [81]

Table 3 Vibrational frequencies of adsorbed atomic species at their most stable site on Ni(111).

Adsorbate	Calculated (cm^{-1})	Experimental (cm^{-1})
H (fcc)	1142	1100[a], 1170[b]
C (hcp)	586	
N (fcc)	589	403[c], 490[d]
O (fcc)	523	580[e], 560 – 570[f]
S (fcc)	356	410[g]

[a] HREELS [31]
[b] HREELS [32]
[c] HREELS [177]
[d] HREELS [121]
[e] HREELS [66]
[f] HREELS [67]
[g] HREELS [79]

Table 4 Estimated diffusion barriers of adsorbed species on Ni(111).

Adsorbate	Diffusion barrier (eV)		Diffusion path
	PW91	RPBE	
H[a]	0.14	0.14	fcc-bridge-hcp
C[b]	0.66	0.63	hcp-bridge-fcc
N[b]	0.76	0.73	fcc-bridge-hcp
O[a]	0.57	0.53	fcc-bridge-hcp
S[a]	0.29	0.27	fcc-bridge-hcp
CH[b]	0.50	0.50	hcp-bridge-fcc
CH_2[a]	0.23	0.16	fcc-bridge-hcp
CH_3[a]	0.16	0.11	fcc-bridge-hcp
CN[a]	0.16	0.14	fcc-bridge-hcp
HCN	0.18	0.12	hcp-bridge
CO	0.12	0.10	hcp-bridge-fcc
NH[b]	0.70	0.67	fcc-bridge-hcp
NH_2	0.71	0.63	bridge-top
NH_3[a]	0.45	0.37	top-bridge-top
N_2	0.30	0.38	top-bridge-top
NO[a]	0.29	0.25	fcc-bridge-hcp
HCO	0.16	0.12	bridge-top
COH[a]	0.30	0.29	hcp-bridge-fcc
HNO	0.43	0.34	bridge-top
NOH[b]	0.77	0.73	fcc-bridge-hcp
OH	0.09	0.04	fcc-bridge-hcp

[a] Energy was calculated by fixing x and y coordinates of the atom through which the adsorbate binds (e.g. for NO, only the x and y coordinates of N were fixed).
[b] Energy was calculated by fixing x and y coordinates of the atom through which the adsorbate binds (e.g. for NH, only the x and y coordinates of N were fixed), and all coordinates of slab atoms.

Table 5 Geometric parameters of adsorbed species on Ni(111).

Adsorbate	$Z_{A\text{-}Ni}$ (Å)	ΔZ_{Ni} (Å)	$d_{Ni\text{-}Ni}$ (Å)	$d_{A\text{-}B}$ (Å)
H (fcc)	0.911	0.016	2.504	
C (hcp)	0.969	0.059	2.555	
N (fcc)	0.991	0.079	2.531	
O (fcc)	1.110	0.056	2.550	
S (fcc)	1.564	0.030	2.551	
CH (hcp)	1.125	0.061	2.528	1.101
CH_2 (fcc)	1.286	0.049	2.507	1.132
CH_3 (fcc)	1.561	0.037	2.486	1.117
CN (fcc)	1.367	0.027	2.512	1.202
HCN (hcp-fcc)	1.395 ($Z_{C\text{-}Ni}$) 1.286 ($Z_{N\text{-}Ni}$)	0.029	2.479	1.101 (H–C), 1.324 (C–N)
CO (hcp)	1.311	0.051	2.496	1.197
NH (fcc)	1.103	0.068	2.553	1.026
NH_2 (br[a])	1.485	0.130	2.477	1.025
NH_3 (top)	2.039	0.145	2.494	1.026
N_2 (top)	1.807	0.191	2.499	1.135
NO (fcc)	1.194	0.073	2.508	1.223
HCO (br-tilted)	1.493	0.051	2.434	1.110 (H–C), 1.293 (C–O)
COH (hcp)	1.158	0.061	2.516	1.341 (C–O), 0.988 (O–H)
HNO (br-tilted)	1.434	0.068	2.443	1.034 (H–N), 1.372 (N–O)
NOH (fcc)	1.093	0.078	2.543	1.408 (N–O), 0.989 (O–H)
OH (fcc)	1.328	0.043	2.548	0.979

See Figure 1 for definition of listed geometric parameters. The equilibrium $d_{Ni\text{-}Ni}$ for clean Ni(111) exposed to vacuum is 2.488 Å.

[a] br is the abbreviation for bridge.

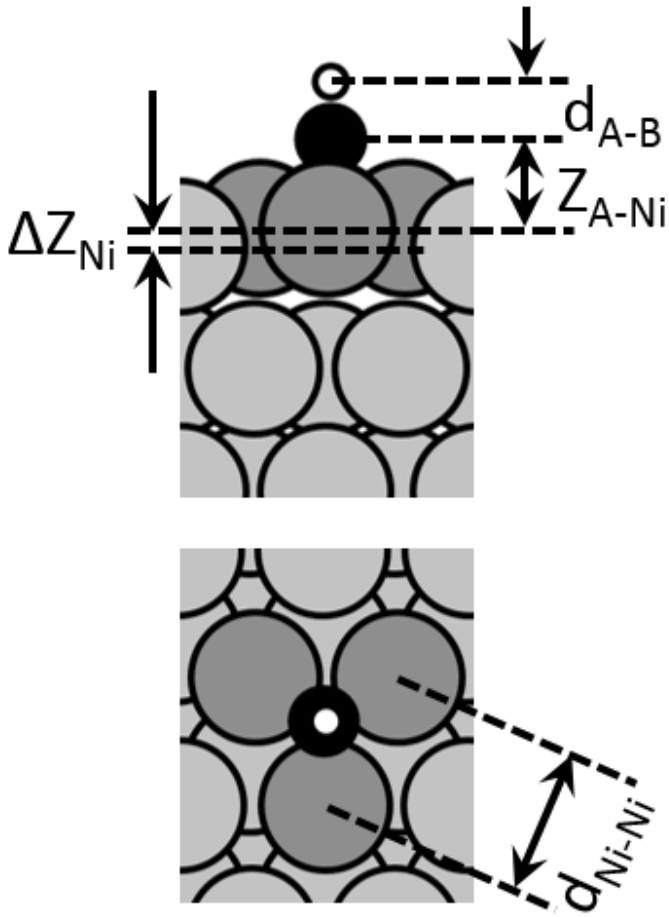

Figure 1 Side and top views of species adsorbed on Ni(111). Definitions of geometric parameters reported in Table 5 are illustrated in the scheme. ΔZ_{Ni} (Å) indicates the change in vertical distance between the plane of Ni atoms in contact with the adsorbate and the plane of a clean Ni slab. d_{A-B} (Å) is the bond length between atoms A and B within an adsorbate. Z_{A-Ni} (Å) indicates the vertical distance between the adsorbate and the plane of the Ni atoms in contact with it. d_{Ni-Ni} (Å) corresponds to the distance between two adjacent Ni atoms in contact with the adsorbate.

Table 6 Calculated deformation energy (ΔE) upon adsorption of each species at its most stable site on Ni(111).

Adsorbate	Site	ΔE (eV)	
		PW91	RPBE
H	fcc	0.01	0.00
C	hcp	0.08	0.06
N	fcc	0.09	0.05
O	fcc	0.08	0.06
S	fcc	0.04	0.02
CH	hcp	0.06	0.03
CH_2	fcc	0.04	0.02
CH_3	fcc	0.04	0.03
CN	fcc	0.02	0.01
HCN	hcp-fcc	0.09	0.07
CO	hcp	0.03	0.01
NH	fcc	0.08	0.05
NH_2	br	0.15	0.13
NH_3	top	0.07	0.06
N_2	top	0.11	0.10
NO	fcc	0.07	0.04
HCO	br-tilted	0.08	0.06
COH	hcp	0.06	0.03
HNO	br-tilted	0.12	0.10
NOH	fcc	0.10	0.07
OH	fcc	0.09	0.09

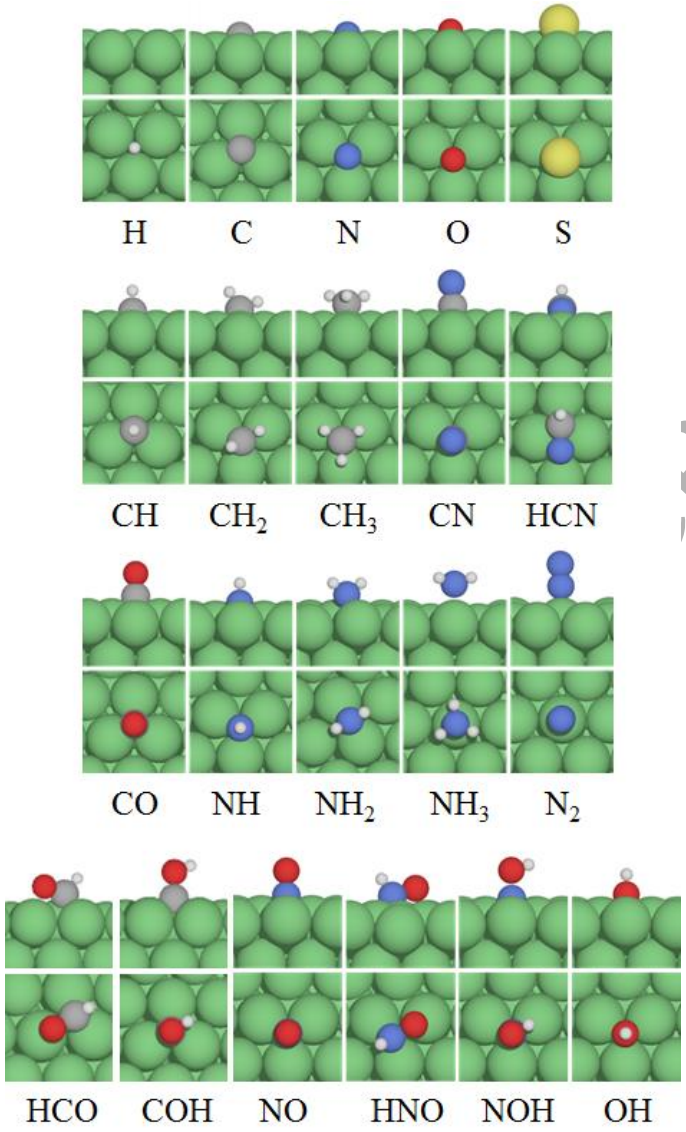

Figure 2 Side view and top view of most stable adsorption structures for adsorbates on Ni(111). Geometric details of these structures are summarized in Table 5.

3.1 Adsorption of atomic species

Hydrogen

Hydrogen binds at fcc (see Figure 2) and hcp sites practically isoenergetically, with calculated PW91 [RPBE in brackets] binding energies of -2.89 [-2.72] eV and -2.88 [-2.71] eV, respectively. Our calculated energetics are in good agreement with previous theoretical results

[34, 35, 43, 178, 179]. For direct comparison with available experimental data, we also calculate the heat of adsorption for a single H atom with respect to gas-phase hydrogen (1/2 H_2): -0.61 [-0.43] eV and -0.60 [-0.42] eV, for the fcc and hcp sites, respectively. Using flash desorption spectroscopy, Lapujoulade et al. determined the adsorption energy of 1/2 H_2 to be -0.49 eV at room temperature [176], and a similar value of -0.50 eV was reported in a later study employing the same technique [26]. A number of LEED and STM analyses have shown that at the coverage of 0.5 monolayer (ML), H adsorbs in a p(2 × 2)-2H graphitic overlayer structure [27, 29, 33], whereas at higher coverages, a p(1 × 1)-1H phase has been reported [29, 32]. In particular, it has been concluded that in the p(2 × 2)-2H overlayer structure, H atoms prefer both types of three-fold hollow sites, i.e., the fcc and hcp sites [27, 29], which agrees with our calculated H binding site preferences. Previous studies also reported that when Ni(111) is exposed to H_2, two distinct features, i.e., β1 and β2 states, exist, yet the β1 state is only filled after the completion of β2 state [26, 30]. At very high hydrogen pressures (1.1 – 5.4 GPa), the formation of NiH hydride was observed and a two-phase separation was found in studies using X-rays from synchrotron radiation [180, 181]. Our calculation shows that at the most stable fcc site, H resides 0.91 Å above the first Ni layer, with a corresponding Ni–H bond length of 1.71 Å, in excellent agreement with available theoretical data of 1.71 Å [34, 35]. though slightly smaller than the experimental measurements of 1.73 – 1.86 Å [27, 28, 182]. Our calculated vibrational frequency for the fcc-bound H (Ni–H stretching mode) is 1142 cm^{-1}. A HREELS study found an energy loss at 1100 cm^{-1} at the H coverage of 0.50 ML, and 1170 cm^{-1} at the H coverage of 1.0 ML, both corresponding to the H–Ni stretching mode [31-32]. Studies of hydrogen diffusion on Ni(111) determined that at above 110 K, hydrogen diffusion was activated by 18.9 kJ/mol (0.20 eV), while at temperatures below 110 K, this process had a smaller activation energy of 10.1

kJ/mol (0.10 eV) [183]. We estimate a diffusion barrier from the fcc to hcp site of 0.14 [0.14] eV, which falls into the experimentally determined range. The adsorption of hydrogen only slightly deforms the Ni(111) surface, with a deformation energy of 0.01 [0.00] eV.

Carbon

Carbon binds to Ni(111) the most strongly among all the atomic species studied in this work. Carbon atoms adsorb at the fcc and hcp (see Figure 2) sites nearly isoenergetically, with binding energies of -6.54 [-6.03] eV and -6.56 [-6.04] eV, respectively. Our calculated binding energies and site preferences are in good agreement with previous theoretical studies [6, 52, 53]. Experimentally, two forms of carbon have been identified, and are distinguished by their Auger-line shape. At temperatures below 600 K, the carbidic carbon forms and is considered as the active carbon that participates into catalytic reactions, while at temperatures above 700 K, the graphitic carbon forms, which is responsible for poisoning Ni catalysts [48]. It has also been widely accepted that at high C coverages (>0.45 ML), Ni(111) undergoes a reconstruction [48, 49], which leads to complex adsorption phases of C. Using LEED and STM, Klink et al. found that in the carbidic phase, surface Ni atoms rearrange into a "clock" reconstruction with an almost square ~ 5 × 5 $Å^2$ (2 × 2)-2C surface mesh [48]. Further, previous LEED studies determined C-induced reconstructions of Ni(111): the c(5√3 × 9)rect structure [49] and the (√39 × √39) structure [50].

We find that at the most stable hcp site, C atom is 0.97 Å above the first Ni layer, with a C–Ni bond length of 1.77 Å, in accordance with published calculated values of 1.77 – 1.78 Å [52, 53]. The C–Ni stretching mode is calculated at 586 cm^{-1}, and the diffusion barrier from the hcp to fcc site is estimated to be 0.66 [0.63] eV.

Nitrogen

Atomic nitrogen binds to fcc (see Figure 2) and hcp sites of Ni(111), with binding energies of -5.01 [-4.53] eV and -4.98 [-4.49] eV, respectively. These values are in good agreement with a previous DFT study [130]. Past LEED and HREELS studies suggest that adsorption of N on Ni(111) would lead to a surface reconstruction and generate the Ni(111)-c($5\sqrt{3} \times 9$)rect structure, similar to what has been found for C and S adsorption on Ni(111) [49, 177]. When N adsorbs at the fcc site, the surrounding Ni atoms are displaced by 0.08 Å above their pristine position and the Ni–Ni bond length is expanded by 0.04 Å. Those changes to the Ni(111) surface cost a deformation energy of 0.09 [0.05] eV. We calculate the N–Ni stretching mode vibrational frequency at 589 cm^{-1}. Due to the surface reconstruction, it has remained a challenge to measure the N–Ni(111) stretching mode experimentally on the unreconstructed surface. A HREELS study indicated an energy loss at 50 meV (403 cm^{-1}), which was assigned to the N–Ni vibrational mode for the reconstructed surface [177]. The diffusion barrier from the fcc to hcp site is estimated to be 0.76 [0.73] eV.

Oxygen

Atomic oxygen adsorbs at fcc (see Figure 2) and hcp sites with binding energies of -5.13 [-4.52] eV and -5.02 [-4.42] eV, respectively, with respect to atomic oxygen in the gas phase. If molecular oxygen is used as the reference state, these numbers correspond to 1/2 O_2 dissociative heat of adsorption of -2.31 [-1.92] eV and -2.20 [-1.82] eV, respectively. Our calculated results are in reasonable agreement with previous theoretical studies [53, 69, 70]. Using single-crystal adsorption calorimetry, Stuckless et al. found the initial heat of adsorption of 1/2 O_2 on Ni(111) to be 220 kJ/mol (2.28 eV) [64]. Two ordered phases, the p(2 × 2) at O coverage of 0.25 ML [47,

55, 59, 60, 62, 63, 65, 66, 68, 184] and the (√3x√3)R30° at O coverage of 0.33 ML [47, 55, 58, 60, 62, 63, 66, 184], have been identified experimentally. A LEED study of the p(2 × 2) structure found that O atoms reside on three-fold hollow sites, with a perpendicular distance of 1.17 Å above the first Ni layer, corresponding to a Ni–O bond length of 1.88 Å [57]. However, the preference between the two three-fold sites was not determined in this LEED study. A subsequent NEXAFS study indicated that only one type of site is occupied, and the fcc site is preferred over the hcp site [60]. A Ni–O bond length of 1.85 Å was reported in the same work, which is quite close to our calculated value of 1.84 Å, corresponding to a 1.11 Å vertical distance of the O atom from the first Ni layer. Another LEED study reported a similar Ni–O bond length of 1.83 Å and indicated that the three surface Ni atoms around the adsorbed O atom are lifted up vertically by about 0.12 Å [59]. Our calculations show that the surface Ni atoms to which O directly binds protrude by 0.06 Å, and the distance between them is increased by 0.06 Å, leading to a deformation energy of 0.08 [0.06] eV. An EELS study of the p(2 × 2) phase found that the O–Ni stretching mode is at 580 cm^{-1} [66], whereas HREELS identified this vibrational feature at 560 – 570 cm^{-1} [67], in reasonable agreement with our calculated stretch at 523 cm^{-1}. We estimate a diffusion barrier from the fcc to hcp site of 0.57 [0.53] eV.

Sulfur

Sulfur atoms adsorb at the fcc (see Figure 2) and hcp sites with binding energies of -5.12 [-4.62] eV and -5.07 [-4.57] eV, respectively. Our calculated values are in good agreement with available theoretical results [82-84]. A number of adsorption phases have been observed experimentally. In particular, a (√39 × √39) structure was reported at a S coverage of 0.22 ML [71, 74]; a p(2 × 2) structure was found at a S coverage of 0.25 ML [73, 75-78, 81]; a (√3 × √3)R30° structure was found at a S coverage of 0.33 ML [71, 74, 76]. At higher coverages, more

complex patterns, including a (5√3 × 2)rect structure at a coverage of 0.4 ML [47, 49, 71, 72, 74, 76, 78-80], and a (8√3 × 2)rect structure at a coverage of 0.44 ML [71], were observed. An early LEED study of the p(2 × 2) structure concluded that at the coverage of 0.25 ML, S prefers to bind at the fcc hollow sites, with a S–Ni bond length of 2.02 Å [75]. The fcc site preference of S at the 0.25ML coverage was confirmed by later analysis using NIXSW [76], ICISS [81], and LEED [77], though slightly longer S–Ni bond lengths (2.10 – 2.16 Å) were reported in these studies. For the fcc site, our calculations indicate that S binds 1.56 Å above the first surface Ni layer, corresponding to a 2.15 Å S–Ni bond length, in reasonable agreement with these experimental measurements. Using HREELS, for the p(2 × 2) structure, Mullins et al. found a characteristic S–Ni mode at 410 cm^{-1} [79]. They also indicated that with increasing S coverage, the S–Ni stretching mode shifts to lower frequencies (325 cm^{-1} at coverage of 0.4 ML). The calculated S–Ni vibrational mode is 356 cm^{-1}. The diffusion barrier for path fcc-bridge-hcp is estimated to be 0.29 [0.27] eV.

Table 7 Binding energies in PW91 [RPBE in brackets] for stable sites and site preference of molecular species and molecular fragments on Ni(111), and average magnetic moment per surface Ni atom (that binds directly to the adsorbate). Reference state is the adsorbate in the gas phase at infinite separation from the slab. For comparison, the magnetic moment per surface Ni atom in the clean relaxed slab is $0.68\mu_B$.

	Preferred Site		Binding Energy (eV)					Magnetic moment per surface Ni atom (μ_B)			
	Calc.	Exp.	top	bridge	fcc	hcp	Exp.	top	bridge	fcc	hcp
CH	hcp	hollow[a]			-6.27	**-6.28**					
					[-5.68]	**[-5.68]**				0.19	0.19
CH_2	fcc		-2.84		**-3.89**	-3.86					
			[-2.40]		**[-3.32]**	[-3.30]		0.26		0.35	0.36
CH_3	fcc	hollow[a]	-1.60		**-1.84**	-1.83	-2.26[b]				
			[-1.26]		**[-1.34]**	[-1.33]		0.34		0.52	0.52
CN	fcc				**-3.95**	-3.93					
					[-3.52]	[-3.50]				0.50	0.50
HCN	hcp-fcc		-0.93	-1.24	-1.38	**-1.42**					
			[-0.39]	[-0.60]	[-0.69]	**[-0.72]**		0.30	0.33	0.39	0.38
CO	hcp	hollow[c]	-1.61	-1.87	-1.97	**-1.99**	-1.20[d],				
			[-1.28]	[-1.48]	[-1.57]	**[-1.58]**	-1.32[e]	0.25	0.29	0.35	0.34

NH	fcc				**-4.44**	-4.36				
					[-3.82]	[-3.74]			0.34	0.34
NH_2	br		-1.96	**-2.68**						
			[-1.52]	**[-2.14]**				0.47	0.48	
NH_3	top	top[f]	**-0.59**				-0.74[g],			
			[-0.23]				-0.77[h]	0.55		
N_2	top		**-0.48**	-0.18	-0.13	-0.12	-0.52[i],			
			[-0.13]	[0.25]	[0.34]	[0.35]	-0.36[j]	0.35	0.36	0.40	0.39
NO	fcc	hollow[k]	-1.53		**-2.49**	-2.47	-1.08[l]			
			[-1.07]		**[-1.89]**	[-1.86]		0.21		0.22	0.21
HCO	br-tilted		-2.21	**-2.37**	-1.99	-1.98				
			[-1.67]	**[-1.79]**	[-1.43]	[-1.45]		0.35	0.32	0.48	0.51
COH	hcp				-4.42	**-4.43**				
					[-3.84]	**[-3.85]**				0.20	0.20
HNO	br-tilted		-2.14	**-2.57**						
			[-1.54]	**[-1.88]**				0.54	0.30		
NOH	fcc				**-3.24**	-3.17				
					[-2.56]	[-2.48]				0.18	0.19
OH	fcc		-2.47	-2.92	**-3.01**	-2.91	-3.27[m]			
			[-2.01]	[-2.37]	**[-2.40]**	[-2.31]		0.48	0.59	0.62	0.66

Numbers in bold indicate the binding energies of species at the most stable site.

[a] HREELS [89]

[b] Single-crystal adsorption calorimetry [185]

[c] LEED [100]

[d] TPD [107]

[e] TPD [99]

[f] PhD [128]

[g] ESDIAD and TPD [127]

[h] TPD [124]

[i] Adsorption isotherms measurements [114]

[j] Isothermal IRAS [116]

[k] LEED, SXPS and PhD [145], LEED [146, 186], SEXAFS [151], NEXAFS [150]

[l] Flash desorption spectroscopy [138], TDS [139]

[m] Single-crystal adsorption calorimetry [205]

3.2 Adsorption of molecules and molecular fragments

CH, CH_2, and CH_3

CH adsorbs at the fcc and hcp sites with binding energies of -6.27 [-5.68] eV and -6.28 [-5.68] eV, respectively. Stable adsorption configurations of CH_2 at top, fcc, and hcp sites are found, with binding energies of -2.84 [-2.40] eV (top), -3.89 [-3.32] eV (fcc), and -3.86 [-3.30] eV (hcp), respectively. Similar to CH_2, CH_3 is also stable at top, fcc, and hcp sites, with binding energies of -1.60 [-1.26] eV, -1.84 eV [-1.34] eV, and -1.83 [-1.33] eV, respectively. Using single-crystal

adsorption calorimetry, Carey et al. measured the CH_3-Ni(111) bond enthalpy at 0.04 ML coverage and reported a value of -2.26 eV [185]. Compared to the experimental value, our DFT results show weaker binding for CH_3, likely due to the higher coverage (0.25 ML) employed in the calculations.

Previous theoretical analyses concluded that three-fold sites are preferred for all CH_x species, and that the interaction strength between CH_x and Ni(111) decreases in the order of CH > CH_2 > CH_3 [6, 91-93]; both agree with our calculated results. CH is bound to the hcp site (see Figure 2), 1.13 Å above the first Ni layer, with a C–H bond length of 1.10 Å. The interacting Ni atoms are lifted by 0.06 Å with an associated deformation energy of 0.06 [0.03] eV. CH_2 binds to the fcc site (see Figure 2) with a vertical distance of 1.29 Å from the first Ni layer. One of the C–H bonds in the CH_2 points to a top site, 69° away from the surface normal, while the other C–H bond points to a bridge site, 33° away from the surface normal. The two C–H bond lengths are 1.16 and 1.10 Å, respectively. At the fcc site (see Figure 2), CH_3 is bound 1.56 Å above the first Ni layer, corresponding to a Ni–C bond length of 2.12 Å, with C–H bond lengths of 1.12 Å. The three Ni atoms that CH_3 binds to are slightly pulled up by 0.04 Å with an associated deformation energy of 0.04 [0.03] eV.

For CH at the hcp site, the calculated C–H stretching mode is at 3039 cm^{-1} and the C–Ni mode is at 615 cm^{-1}. In a HREELS study of CH_3 vibrational modes, Yang et al. found that adsorbed CH_3 begins to decompose into CH when the surface temperature is increased to 150 K [89]. They assigned the energy loss at 2970 cm^{-1} to the C–H stretching mode and the vibrational loss feature at 650 cm^{-1} to the C–Ni stretching mode, both in reasonable agreement with our calculated values. Another HREELS study suggested the C–H stretching mode at 2980 cm^{-1} [88]. We estimate a 0.50 [0.50] eV diffusion barrier for CH to move from the hcp to the fcc site.

For CH_2 at the fcc site, we obtain two C–H stretching modes at 2411 cm^{-1} and 3013 cm^{-1}, a C–Ni mode at 489 cm^{-1}, a wagging mode at 678 cm^{-1}, a scissoring mode at 1396 cm^{-1}, a twisting mode at 294 cm^{-1}, and a rocking mode at 564 cm^{-1}. A limited set of experimental data on CH_2 adsorption on Ni(111) is available for direct comparison. Using HREELS, Demuth et al. proposed a scissoring mode at 1300 cm^{-1} [88], which is close to our calculated value of 1396 cm^{-1}. The estimated diffusion barrier for CH_2 to move from fcc to hcp is 0.23 [0.16] eV.

For CH_3 at the fcc site, we obtain a C–H symmetric stretching mode at 2798 cm^{-1}, C–H asymmetric stretching modes at 2866 – 2870 cm^{-1}, a C–Ni stretching mode at 354 cm^{-1}, a symmetric deformation mode at 1155 cm^{-1}, scissoring (asymmetric deformation) modes at 1296 – 1300 cm^{-1}, a twisting mode at 378 cm^{-1}, and rocking modes at 468 – 481 cm^{-1}. Using HREELS, Yang et al. analyzed the vibrational behavior of CH_3 that is generated from CH_4 dissociation at very low coverage (no greater than 0.1 ML) [89]. They identified a C–H symmetric stretching mode at 2655 cm^{-1}, doubly degenerate asymmetric stretching modes at 2730 cm^{-1}, a C–Ni stretching mode at 385 cm^{-1}, a symmetric deformation mode at 1220 cm^{-1}, a doubly degenerate asymmetric deformation at 1320 cm^{-1}, a torsional rotation mode at 485 cm^{-1}, and a rocking mode at 965 cm^{-1}. Except the rocking mode, the rest of the calculated modes are in good agreement with experiment. We estimate a diffusion barrier of 0.16 [0.11] eV for CH_3 to move from the fcc to the hcp site.

Table 8 Vibrational frequencies (in cm^{-1}) of adsorbed diatomic species on Ni(111) in their preferred adsorption configuration.

Adsorbate	Ni–X		A–B	
	Cal.	Exp.	Calc.	Exp.
CH (hcp)	615	650[a]	3039	2970[a], 2980[b]
CN (fcc)	360		1971	
CO (hcp)	349	400[c]	1866	1810[c], 1817[d]
NH (fcc)	552	620[e]	3472	3340[e]
N_2 (top)	347		2247	2202[f], 2186[g], 2218[h]
NO (fcc)	353		1569	1460-1475[i], 1486[j], 1573[k]
OH (fcc)	434	524[l]	3743	3630[l]

Ni–X refers to nickel–adsorbate (X) stretching mode, while A–B refers to the stretch of the intramolecular mode.

[a] HREELS [89]
[b] HREELS [88]
[c] HREELS [104]
[d] IRAS [98]
[e] HREELS [121]
[f] IR [114]
[g] RAIRS [115]
[h] FT-IRAS [116]
[i] RAIRS [137]
[j] FT-RAIR [142]
[k] HREELS [187]
[l] HREELS [188]

CO

Carbon monoxide is stable adsorbed at top, bridge, fcc, and hcp (see Figure 2) sites of Ni(111) with binding energies of -1.61 [-1.28] eV, -1.87 [-1.48] eV, -1.97 [-1.57] eV, and -1.99 [-1.58] eV, respectively, which agree well with previous DFT results [53, 110, 111]. Using TPD, Beniya et al. estimated that at very low coverages (θ_{CO} < 0.10 ML), the CO desorption energy was 1.2 eV [107], which is very close to values reported from a threshold TPD study [189]. A number of overlayer structures for CO adsorption on Ni(111) have been found with various experimental techniques, including ($\sqrt{3} \times \sqrt{3}$)R30° [96, 97, 109], c(4 × 2) [97, 100-103, 109], and ($\sqrt{7}/2 \times \sqrt{7}/2$)R19.1° [97, 100], corresponding to CO coverages of 0.33 ML, 0.5 ML, and 0.57 ML,

respectively. Using IRAS, combined with AES and TDS, Campuzano et al. found that at low CO coverage (θ_{CO} = 0.05 ML), CO adsorbs at three-fold sites with a stretching frequency of 1817 cm^{-1}, which agrees with our calculated value of 1866 cm^{-1} for CO at the hcp site [98]. They also found that, with increasing coverage, CO starts to bind on the two-fold bridge site and even the top site at the coverage of 0.57 ML. For CO adsorption at the bridge and top sites, they reported the C–O stretching frequencies at 1910 cm^{-1} and 2045 cm^{-1}, respectively. In a HREELS study by Erley et al., a shift of the C–O stretching frequencies from 1810 cm^{-1} to 1910 cm^{-1} and to 2050 cm^{-1} was reported with increasing CO coverage [104]. This shift was attributed to the population of CO on bridge and top sites at high coverage. They also found a characteristic loss peak at 400 cm^{-1} and assigned that to a C–Ni vibrational mode, in reasonable agreement with our calculated value of 349 cm^{-1}. A SEXAFS study of Ni(111)-c(4 × 2)-CO showed that the three-fold hollow site is favorable, at which a C–O bond length of 1.19 Å was measured, and the C atom was about 1.05 Å above the first Ni layer [103]. Our calculated C–O bond length in the most stable CO adsorption structure (hcp) is 1.20 Å, in excellent agreement with that reported value. A LEED study has identified that, in the c(4 × 2) structures, the average C–Ni bond length is 1.89 Å for CO at the hcp site [100], which agrees with our calculated value of 1.95 Å and results from other experimental studies [101, 102]. CO diffusion has been studied by field emission microscopy fluctuation, and a barrier of 6.8 kcal/mol (0.29 eV) was found [190]. We estimate a CO diffusion barrier from the fcc to the hcp site of 0.12 [0.10] eV.

CN and HCN

CN is stable at the fcc and hcp sites of Ni(111) with binding energies of -3.95 [-3.52] eV and -3.93 [-3.50] eV, respectively. In both structures, CN is bound through the C atom, with the N above the C atom and a C–N bond length of 1.20 Å. For CN binding at the fcc site (see Figure 2),

the C atom stands 1.37 Å above the first layer of Ni atoms, corresponding to a C–Ni bond length of 1.99 Å. Our calculated energetic and geometric results agree with previous DFT studies [191-193]. The three Ni atoms that CN binds to protrude out of the surface by 0.03 Å, and the Ni–Ni distance is expanded by 0.02 Å, for an energy cost of 0.02 [0.01] eV. We calculate the C–N stretching mode at 1971 cm^{-1}, and the C–Ni stretching mode at 360 cm^{-1}. A detailed characterization of CN on Ni(111) is not available in the literature, however, EELS measurements of CN adsorption on Pd(111) found a C–N stretching mode at 1910 cm^{-1} [194], which is close to our computed value. Diffusion of CN from the fcc to the hcp site has an estimated barrier of 0.16 [0.14] eV.

HCN binds to Ni(111) with both the C and the N atoms. Several stable adsorption structures are found. In the most stable hcp-fcc structure, the C atom is above an hcp site, whereas the N atom is above an adjacent fcc site, with the C–N bond spanning the bridge site (see Figure 2). In this particular structure, the C–H has a bond length of 1.10 Å and the C–N has a bond length of 1.32 Å. The second most stable structure features the C and N atoms binding to adjacent fcc and hcp sites, respectively. In next most stable configuration, the C and N atoms are bound to adjacent bridge sites. In the least stable structure, the C and N atoms bind to two nearby top sites. The binding energies of HCN in these stable structures are -1.42 [-0.72] eV, -1.38 [-0.69] eV, -1.24 [-0.60] eV and -0.93 [-0.39] eV, respectively. The calculated binding energies are in good agreement with a previous DFT study [195]. In a study using combined scanning kinetic spectroscopy (SKS), TPD, and AES, Hagans et al. found two states of HCN, with desorption energies of 18 kcal/mol (0.78 eV) and 20 kcal/mol (0.87 eV) at 258 K and 271 K, respectively [196]. For HCN in its most stable state, we calculate a C–H stretching mode at 3018 cm^{-1}, a C–N stretching mode at 1301 cm^{-1}, a scissoring mode at 1016 cm^{-1}, a molecule–surface stretching

mode at 450 cm^{-1}, a wagging mode at 732 cm^{-1}, a twisting mode at 228 cm^{-1}, and a rocking mode at 365 cm^{-1}. The diffusion barrier for HCN from the hcp to bridge site is estimated to be 0.18 [0.12] eV.

NH and NH_2

NH adsorbs at the fcc and hcp sites of Ni(111) with binding energies of -4.44 [-3.82] eV, and -4.36 [-3.74] eV, respectively. NH_2 has only two stable structures, at the top and bridge site, with binding energies of -1.96 [-1.52] eV and -2.68 [-2.14] eV, respectively. Our calculated binding energies and site preferences are consistent with a previous DFT study [130]. At the fcc site, NH binds to Ni(111) via the N atom, with the N–H bond axis perpendicular to the surface plane (see Figure 2). The N atom in NH is 1.10 Å above the first Ni layer, corresponding to a Ni–N bond length of 1.84 Å, and the N–H bond length is 1.03 Å. Adsorption of NH induces a 0.07 Å protrusion of the three contacting Ni atoms out of the surface plane, and a 0.07 Å expansion in the nearest Ni–Ni distance. The associated deformation energy is 0.08 [0.05] eV. Adsorbed NH with the N–H bond axis oriented perpendicular to the surface has been found as a stable intermediate during hydrazine decomposition on Ni(111) in the temperature range of 285 to 365 K [121]. At the bridge site, the most stable state for NH_2 (see Figure 2), NH_2 is bound through the N atom, which is 1.49 Å above the first Ni layer. Both N–H bonds in NH_2 are 1.03 Å in length, and the H–N–H angle is 109°. The two Ni atoms that NH_2 binds to are pulled out of the surface plane by 0.13 Å, leading to the greatest deformation energy among all species studied here, 0.15 [0.13] eV. A HREELS study of NH identified an N–H stretching mode at 3340 cm^{-1} and a Ni–NH stretching mode at 620 cm^{-1} [121]. For NH at the fcc site, we obtain an N–H stretching mode at 3472 cm^{-1} and a Ni–NH stretching mode at 552 cm^{-1}. For NH_2 at the bridge site, vibrational modes are found at 3429 cm^{-1} for N–H symmetric stretching, 3531 cm^{-1} for N–H

asymmetric stretching, 614 cm^{-1} for wagging, 1482 cm^{-1} for scissoring, 584 cm^{-1} for twisting, 618 cm^{-1} for rocking, and 465 cm^{-1} for Ni–N stretching. The estimated diffusion barriers for NH (fcc-bridge-hcp) and NH_2 (bridge-top) are 0.70 [0.67] eV and 0.71 [0.63] eV, respectively.

Table 9 Vibrational frequencies (in cm^{-1}) of adsorbed polyatomic species on Ni(111) in their preferred adsorption configuration.

	CH_2	CH_3		HCN	NH_2	NH_3		HCO	COH	HNO	NOH
	fcc	fcc	Exp.	hcp-fcc	br-tilted	top	Exp.	br-tilted	hcp	br-tilted	fcc
Symmetric IM stretch		2798	2655[a]		3429	3367	3270[b] 3251[c]				
Asymmetric IM stretch	3013 2411	2870 2866	2730[a]	3018 (C–H) 1301 (C–N)	3531	3523 3525	3360[b]	2916 (C–H) 1317 (C–O)	3693 (O–H) 1273 (C–O)	3453 (N–H) 981 (N–O)	3690 (O–H) 878 (N–O)
AS stretch	489	354	385[a]	450	465	280		479	394	453	392
Symmetric deformation		1155	1220[a]			1019	1140[b] 1113[c]				
Wagging	678			732	614			625	403	522	471
Scissoring	1396	1296 1300	1320[a]	1016	1482	1545 1543	1580[b]	1164	1116	1084	1260
Twisting	294	378	485[a]	228	584	101		232	124	255	
Rocking	564	468 481	965[a]	365	618	507 505		319	402	343	429

IM stands for intramolecular, while AS stands for adsorbate-surface.
[a] HREELS [89]
[b] HREELS [125]
[c] FTIR [129]

NH_3

NH_3 binds only at the top site of Ni(111) through its N atom in a tetrahedral structure (see Figure 2) with a binding energy of -0.59 [-0.23] eV. In this particular binding geometry, the N atom is 2.04 Å above the first surface layer, and the N–H bonds are oriented 71° away from the surface normal with equal lengths of 1.03 Å each. The Ni atom that NH_3 binds to is pulled out of the surface plane by 0.15 Å, leading to a deformation energy of 0.07 [0.06] eV. Previous theoretical studies also identified the top site as the preferred site for NH_3 on Ni(111) [112, 130, 132, 133].

Earlier LEED [122-124], TDS [123, 124, 126], UPS [122], TPD [122], ESDIAD [122, 124], and SPIES [126] studies concluded that at low temperatures, NH_3 adsorbs on Ni(111) via the N atom with three H atoms pointing away from the surface, and that NH_3 can desorb molecularly from the surface. However, no site preference was assigned in these studies. Using scanned energy mode PhD, Schindler et al. found that NH_3 preferentially binds to the top Ni(111) site with the Ni–N bond length of 1.97 Å [128]. Using ESDIAD and TPD, Dresser et al. estimated an -0.74 eV binding energy of NH_3 on Ni(111) at very low coverage [127]. and a very similar value (-0.77 eV) was obtained in another TPD study by Netzer and Madey [124]. Several adsorption states have been found for NH_3: monolayer adsorption (α-state), second layer adsorption (β-state), and multilayer regime (γ-state) [124, 125, 131]. A TDS study revealed that NH_3 in the α-state features a desorption peak in the temperature range of 150 – 300 K, while in the β-state, NH_3 desorbs at ~120 K, and an even lower desorption temperature was observed for the γ-state NH_3 [124]. Using HREELS, Fisher and Mitchell studied the vibrational characteristics of NH_3 on Ni(111) and identified a symmetric N–H mode at 3270 cm^{-1}, asymmetric N–H stretching modes at 3360 cm^{-1}, a symmetric bending mode at 1140 cm^{-1}, and asymmetric bending modes at 1580 cm^{-1}.[125] An FTIR study by Xu et al. determined vibrational modes at 3251 cm^{-1} and 1113 cm^{-1}, which were assigned to symmetric N–H stretching and symmetric deformation, respectively [129]. We obtain a number of vibrational modes for adsorbed NH_3, including a symmetric N–H stretching mode at 3367 cm^{-1}, asymmetric N–H stretching modes at 3523 – 3525 cm^{-1}, a symmetric deformation mode at 1019 cm^{-1}, scissoring modes at 1543 – 1545 cm^{-1}, a twisting mode at 101 cm^{-1}, rocking modes at 505 – 507 cm^{-1}, and a Ni–N stretching mode at 280 cm^{-1}. The diffusion barrier between adjacent top sites is estimated to be 0.45 [0.37] eV.

N_2

N_2 binds the most strongly at the top site (see Figure 2), with a binding energy of -0.48 [-0.13] eV. Though stable N_2 adsorption structures on bridge, fcc, and hcp sites are found, these binding states are less favorable with binding energies of -0.18 [0.25] eV, -0.13 [0.34] eV, and -0.12 [0.35] eV, respectively. In all cases, N_2 binds with the N–N bond axis perpendicular to the surface. Adsorption of N_2 on Ni(111) at low temperatures has been observed experimentally [115, 116, 118]. Hardeveld and Montfoort measured adsorption isotherms and determined that the initial heat of adsorption is about 12 kcal/mol (0.52 eV) at low coverages, which decreases with increasing coverage [114]. Through isothermal IRAS measurements, Yoshinobu et al. estimated the adsorption enthalpy of N_2 on Ni(111) to be -8.4 kcal/mol (-0.36 eV) at zero coverage [116]. At the top site, the calculated N–Ni and N–N bond lengths are 1.81 Å and 1.14 Å, respectively. The Ni atom that N_2 binds to protrudes 0.19 Å from its equilibrium position with an associated deformation energy of 0.11 [0.10] eV. Two overlayer structures have been observed in LEED studies, including p(2 × 2) [115] and (√3 × √3)R30° [116]. An IR study found a N–N stretching mode at 2202 cm^{-1} for N_2 adsorption on nickel [114], whereas an RAIRS analysis identified an absorption band at 2186 cm^{-1} [115]. An FT-IRAS study found that at very low coverages, there is a single N–N absorption band at 2218 cm^{-1}, while with increasing N_2 pressure, two other absorption bands at 2212 – 2208 cm^{-1} and 2204 – 2203 cm^{-1} develop [116]. In our calculations, we observe an N–N stretching mode at 2247 cm^{-1} and a Ni–N stretching mode at 347 cm^{-1}, in good agreement with available experimental data. Diffusion between adjacent top sites is estimated to have a barrier of 0.30 [0.38] eV.

NO

NO adsorbs strongly at the fcc (see Figure 2) and hcp sites of Ni(111) with binding energies of -2.49 [-1.89] eV and -2.47 [-1.86] eV, respectively. A stable adsorbed structure at the top site is

also found, but with a much weaker interaction, characterized by a binding energy of -1.53 [-1.07] eV. On all sites, NO is bound to Ni(111) through the N atom with the N–O bond axis parallel to the surface normal. On all sites, the remaining magnetic moment of NO is very small (i.e., less than 0.1 μ_B). At the fcc site, the most stable binding site for NO, the N atom is 1.19 Å above the surface Ni layer, with an N–O bond length of 1.22 Å. The three Ni atoms surrounding the N atom are pulled upwards by 0.07 Å, and the distance between them is increased by 0.02 Å, with an associated deformation cost of 0.07 [0.04] eV. An ESDIAD study of NO adsorption at 80 K revealed that NO is bound perpendicular to Ni(111), which agrees with our results, though the site preference was not determined in that work [136]. A combined LEED, SXPS, and PhD study found that NO preferentially adsorbs at both the fcc and hcp three-fold hollow sites in a ratio of approximately 1:1 with Ni–N bond lengths of 1.83 Å (fcc) and 1.85 Å (hcp) [145]. The N–O bond length at the fcc site was found to be 1.18 Å [145]. The preference for hollow sites was confirmed by many other studies using LEED [146, 186], SEXAFS [151], and NEXAFS [148], and Ni–N bond lengths of 1.82 – 1.93 Å were reported for NO at these sites. Our calculated results agree well with these experimental findings. Using flash desorption spectroscopy, Conrad et al. found an NO desorption barrier of about 25 kcal/mol (1.08 eV) [138], which was confirmed by a later TDS study by Bozso et al. [139] The well-known c(4 × 2) structure has been extensively characterized with LEED [72, 138, 143, 145, 147-149, 186] and SEXAFS [103]. A RAIRS study observed a single absorption band at 1460 cm^{-1} at low NO coverages, while with increasing NO coverage, a well-separated band at 1475 cm^{-1} develops [137]. A blue-shift of the N–O stretching mode was observed in other FTIR studies [140, 141, 144], and was attributed to changes of NO binding geometry at high coverages [140, 141]. A FT-RAIR study of NO adsorption identified a single absorption band at 1486 cm^{-1} corresponding to the stretching of the

N–O bond [142], whereas HREELS documented this stretching mode at 195 meV (1573 cm^{-1}) [187]. We obtain a calculated N–O stretching mode at 1569 cm^{-1} and a Ni–N stretching mode at 353 cm^{-1}. The estimated diffusion barrier for NO to move from the fcc to hcp site is 0.29 [0.25] eV.

HCO and COH

HCO and COH are possible surface intermediates for reaction systems such as the Fischer-Tropsch synthesis [197], CO methanation [198], and methanol synthesis [199]. HCO prefers to adsorb at a bridge site on Ni(111) through a tilted configuration, in which the C atom binds at a bridge site, and the O atom is tilted towards an adjacent top site with the C–O bond above an hcp site (see Figure 2). The binding energy of this bridge-tilted structure is -2.37 [-1.79] eV. There also exists an isoenergetic bridge-tilted structure in which the C–O bond is located above an fcc site instead of an hcp site. We observe less stable binding structures of HCO at top, fcc, and hcp sites with binding energies of -2.21 [-1.67] eV, -1.99 [-1.43] eV, and -1.98 [-1.45] eV, respectively. Over its preferred binding site, HCO sits at a vertical distance of 1.49 Å above the surface with a Ni–C bond length of 1.95 Å and a Ni–O bond length of 1.96 Å; the calculated C–H bond length, C–O bond length, and H–C–O bond angle are 1.11 Å, 1.29 Å, and 116º, respectively. The adsorption of HCO is associated with a surface deformation energy of 0.08 [0.06] eV; upon adsorption, the adjacent surface Ni atoms are drawn upwards by 0.05 Å and closer to each other by 0.05 Å. Several vibrational frequencies are calculated for the most stable binding structure of HCO, namely, a C–H stretching mode at 2916 cm^{-1}, a C–O stretching mode

at 1317 cm^{-1}, a Ni–C stretching mode at 479 cm^{-1}, a wagging mode at 625 cm^{-1}, a scissoring mode at 1164 cm^{-1}, a twisting mode at 232 cm^{-1}, and a rocking mode at 319 cm^{-1}. HCO can diffuse between two adjacent bridge sites through a top site with an estimated diffusion barrier of 0.16 [0.12] eV.

COH prefers to bind at an hcp site with a binding energy of -4.43 [-3.85] eV. Compared to its isomer HCO, COH is 0.30 [0.30] eV more stable when adsorbed on Ni(111). COH can also adsorb at an fcc site with a binding energy of -4.42 [-3.84], only 0.01 [0.01] eV less stable than the hcp binding structure. As shown in Figure 2, COH binds through the C atom with the C–O bond perpendicular to the surface and the O atom tilted towards the surface. At an hcp site, COH lies 1.16 Å vertically above the surface; the calculated C–O bond length, O–H bond length, and H–O–C bond angle are 1.341 Å, 0.988 Å, and 110º, respectively. The adsorption of COH draws the adjacent surface Ni atoms upwards by 0.06 Å and leads to a local lattice expansion by 0.03 Å. Such a surface deformation is associated with an energy of 0.06 [0.03] eV. The calculated vibrational features for the most stable adsorption structure of COH are: an O–H stretching mode at 3693 cm^{-1}, a C–O stretching mode at 1273 cm^{-1}, a Ni–C stretching mode at 394 cm^{-1}, a wagging mode at 403 cm^{-1}, a scissoring mode at 1116 cm^{-1}, a twisting mode at 124 cm^{-1}, and a rocking mode at 402 cm^{-1}. The estimated diffusion barrier of COH is 0.30 [0.29] eV along the following diffusion path: hcp → bridge → fcc.

HNO and NOH

HNO and NOH have been identified as possible intermediates in NO reduction reactions on transition metal surfaces [200-204]. Our calculations indicate that the most stable HNO configuration on Ni(111) features a bridge-tilted structure, in which the N atom binds at a bridge site, and the O atom is oriented towards a top site with the N–O bond lying above an fcc site (see

Figure 2). The binding energy of HNO in this particular structure is -2.57 [-1.88] eV. We find a nearly isoenergetic (with a binding energy of -2.55 [-1.86] eV) configuration, in which the N–O bond lies above an hcp site instead of an fcc site. A much less stable structure with both N and O binding at two adjoining top sites is also found with a binding energy of -2.14 [-1.54] eV. In the most stable structure, we observe a Ni–N bond length of 1.90 Å, a Ni–O bond length of 1.93 Å, an N–H bond length of 1.03 Å, an N–O bond length of 1.37 Å, and a H–N–O angle of 110°. The adsorption of HNO leads to a surface deformation energy of 0.12 [0.10] eV. For the most stable state, a number of vibrational frequencies are calculated, including an N–H stretching mode at 3453 cm^{-1}, an N–O stretching mode at 981 cm^{-1}, a wagging mode at 522 cm^{-1}, a scissoring mode at 1084 cm^{-1}, a twisting mode at 255 cm^{-1}, a rocking mode at 343 cm^{-1}, and a Ni–N stretching mode at 453 cm^{-1}. The diffusion barrier for HNO, 0.43 [0.34] eV, is estimated from the energy difference between the most stable structure and the structure binding to the top site.

NOH adsorbs at the fcc and hcp sites with binding energies of -3.24 [-2.56] eV and -3.17 [-2.48] eV, respectively. Therefore, on Ni(111), the most stable adsorbed NOH is 0.20 [0.22] eV lower in energy (more stable) than its most stable isomer (adsorbed HNO). At the fcc site, NOH binds to the surface through the N atom with the N–O bond axis perpendicular to the surface plane and the H pointing towards a top site (see Figure 2). The most stable configuration has a 1.41 Å N–O bond length, a 0.99 Å O–H bond length, and a 105° N–O–H angle. Ni atoms that are in contact with the N atom are pulled out of the surface layer by 0.04 Å and the Ni–Ni distances are expanded by 0.06 Å, costing a 0.10 [0.07] eV deformation energy. For the fcc bound NOH, we find an O–H stretching mode at 3690 cm^{-1}, an N–O stretching mode at 878 cm^{-1}, a wagging mode at 471 cm^{-1}, a scissoring mode at 1260 cm^{-1}, a rocking mode at 429 cm^{-1}, and a Ni–N

stretching mode at 392 cm^{-1}. We estimate the diffusion barrier for NOH moving from the fcc to hcp site to be 0.77 [0.73] eV.

OH

Stable adsorption structures of OH at top, bridge, fcc, and hcp sites are found, with binding energies of -2.47 [-2.01] eV, -2.92 [-2.37] eV, -3.01 [-2.40] eV, and -2.91 [-2.31] eV, respectively. The PW91 binding energy of OH at the most stable binding site (fcc, -3.01 eV) is in reasonable agreement with the calorimetrically measured value of -3.27 eV at ~0.5 ML by Zhao and co-workers [205]. In the most stable binding structure, OH binds to the surface through the O atom (see Figure 2), with an O–H bond length of 0.98 Å. The O atom is located 1.33 Å above the surface Ni layer, corresponding to a Ni-O bond length of 1.98 Å. Our calculated results are in good agreement with previous theoretical studies [206-209]. The Ni atoms defining the preferred OH adsorption site protrude from their equilibrium positions by 0.04 Å, leading to a deformation energy of 0.09 [0.09] eV. Shan et al. identified OH on Ni(111) using HREELS, AES, and TPD, and found two different methods that may generate OH from H_2O [188]. The first is to anneal H2O on atomic-O pre-covered Ni(111) at 85 K to above 170 K, and the second is to expose pure H_2O to 20 eV electrons at temperatures below 120 K. Based on their analysis, three-fold hollow sites are preferred by OH. They assigned the 450 meV (3630 cm^{-1}) feature to the O–H stretching mode and the 65 meV (524 cm^{-1}) feature to the Ni–OH stretching mode. We calculate an O–H stretching mode at 3743 cm^{-1}, and a Ni–O stretching mode at 434 cm^{-1}. The diffusion of OH from the fcc site to an adjacent hcp site (across a bridge site) has an estimated barrier of 0.09 [0.04] eV.

Adsorbate-Induced Demagnetization of Surface Ni

For each atom, molecule, or molecular fragment, we calculate the average magnetic moment of the Ni atoms that are directly in contact with the adsorbate. Most of these values, as listed in Tables 2 and 7, are much smaller compared to our calculated magnetic moment of a Ni atom in the bulk (0.73 μ_B) or on the clean, relaxed surface (0.68 μ_B). This adsorbate-induced demagnetization effect has been reported in several theoretical studies on Ni surfaces, e.g., CO on Ni(211) [210] and Ni(110) [211], NO on Ni(110) [212], and benzene on Ni(111) [213, 214]. On Ni(110), Jenkins et al. reported that NO causes more pronounced demagnetization than CO [212]. Our results suggest the same trend on Ni(111), as the calculated surface Ni magnetic moments upon NO adsorption (0.21-0.22 μ_B) are smaller than those upon CO adsorption (0.25-0.34 μ_B).

3.3 Thermochemistry for NO, CO, NH_3, N_2, and CH_4 decomposition

Using the calculated PW91 energies of the relevant surface intermediates and gas-phase species, we develop the thermochemical potential energy surfaces for NO, CO, NH_3, N_2, and CH_4 decomposition, as shown in Figure 3.

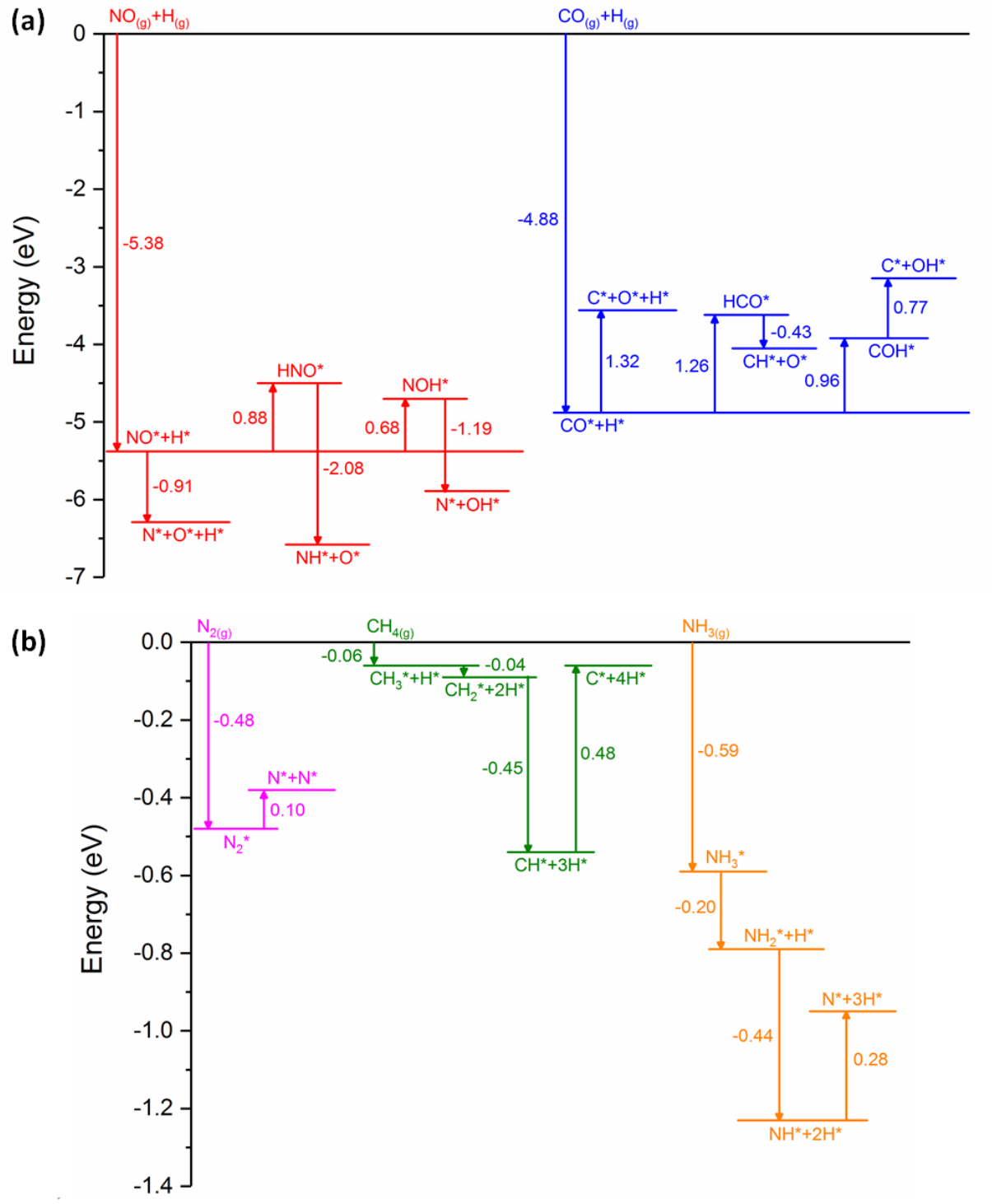

Figure 3 Thermochemistry of molecular decomposition on Ni(111): (a) decomposition of CO and NO; (b) decomposition of N_2, CH_4, and NH_3. The reaction energy for each elementary step is indicated by the number next to the respective arrow.

NO binds to Ni(111) with a binding energy of -2.49 eV, and its decomposition to N* and O* is energetically favorable with a reaction energy of -0.91 eV (see Figure 3(a), red lines). In addition to the direct NO* dissociation, we consider two H-assisted decomposition pathways, in which NO* is hydrogenated to HNO* or NOH* prior to its decomposition into NH* + O* or N* + OH*, respectively. First, we note that both hydrogenation steps are endothermic, which means the formation of HNO* and NOH* are not thermodynamically favorable. Second, the formation of NOH* is 0.20 eV more favorable than HNO*, indicating that NOH* is a more stable species than HNO* on Ni(111). Third, the decomposition of HNO* and NOH* are both exothermic, with reaction energies of -2.08 eV and -1.19 eV, respectively. Finally, the HNO* decomposition products (NH* + O*) have the lowest energy, followed by the complete decomposition products (N* + O* + H*), and NOH* decomposition products (N* + OH*)(see Figure 3(a), red lines).

Similar to NO, CO also adsorbs strongly (-1.99 eV) on Ni(111). However, the decomposition of CO* into C* and O* is endothermic, with a reaction energy of 1.32 eV (Figure 3(a), blue lines). Comparing the desorption and decomposition thermochemistry, we find that the decomposition is 0.67 eV more energetically favorable. We also consider two H-assisted decomposition pathways of CO, in which CO* is hydrogenated to HCO* or COH* prior to its decomposition into CH* + O* or C* + OH*, respectively (Figure 3(a), blue lines). Both the formation steps of HCO* and COH* from CO* + H* are energetically uphill, by 1.26 eV and 0.96 eV, respectively, albeit less endothermic than the direct decomposition of CO*. The formation of COH* is 0.30 eV more favorable than that of HCO*. The subsequent decomposition of COH* into C* + OH*, however, is endothermic by 0.77 eV; on the other hand, the decomposition of HCO* into CH* + O* is exothermic with a reaction energy of -0.43 eV. Overall, the HCO* pathway leads to the

most stable decomposition products (CH* + O*), followed by the direct pathway (C* + O* + H*) and COH* pathway (C* + OH*).

Compared to NO and CO, NH_3 binds to Ni(111) more weakly with a binding energy of -0.59 eV. Three dehydrogenation steps are needed for the complete decomposition of NH_3* into N* and 3H* (see Figure 3(b), orange lines). The first two dehydrogenation steps are slightly exothermic with reaction energies of -0.20 eV and -0.44 eV, respectively, whereas the last N–H bond-breaking step is mildly endothermic (0.28 eV). Considering the overall decomposition process (NH_3(g) + 4 * → N* + 3H*), we find that it is still energetically favorable, with an overall reaction energy of -0.95 eV. Similar to NH_3, N_2 adsorbs on Ni(111) very weakly with a binding energy of -0.48 eV (see Figure 3(b), purple lines) . However, N_2* decomposition (N_2* + * → 2N*) is slightly endothermic (0.10 eV), leading to an overall -0.38 eV decomposition energy with respect to gas phase N_2.

Complete decomposition of CH_4(g) into carbon and hydrogen on Ni(111) is slightly exothermic, with an overall reaction energy of -0.06 eV (see Figure 3(b), green lines). Among the four dehydrogenation steps, the first three are exothermic by -0.06 eV, -0.03 eV and -0.45 eV, respectively, while the last one, CH* + * → C* + H*, is endothermic (ΔE = 0.48 eV). Therefore, based on our computed potential energy surface, CH* might be the most abundant surface intermediate in CH_4 decomposition on Ni, which agrees with previous kinetic model predictions [6].

4 Conclusions

The adsorption properties of atomic species (H, C, N, O, and S), molecular species (CO, HCN, NH_3, N_2, and NO), and molecular fragments (CH, CH_2, CH_3, CN, NH, NH_2, HNO, NOH, and

OH) on Ni(111) are studied using periodic, self-consistent density functional theory (DFT-GGA). We have determined the preferred binding sites, stable adsorption geometries, and binding energies for these species. According to our calculations, the absolute magnitude of the binding energy of these species on Ni(111) decreases in the order of C > CH > O > S > N > NH > COH > CN > CH_2 > NOH > OH > H > NH_2 > HNO > NO > HCO > CO > CH_3 > HCN > NH_3 > N_2. Atomic species prefer to bind at three-fold hollow sites. Surface deformation energies and vibrational frequencies are calculated for the most stable adsorbed state for each species. Comparisons between our calculated results and available literature values show good agreement. Diffusion barriers for each species are also estimated. Finally, the decomposition of NO, CO, NH_3, N_2, and CH_4 is analyzed by constructing the thermodynamic potential energy surfaces, from which we conclude that all these decomposition reactions are preferred to the respective molecular desorption.

Acknowledgements

This work was supported by DOE-BES, Office of Chemical Sciences (Grant DE-FG02-05ER15731). DK was partially supported by a Research Experience for Undergraduate program sponsored by the National Science Foundation (grant number CHE-1262750). We thank T. Szilvasi and S. Li for their comments on this article. Computational work was performed in part using supercomputing resources from the following institutions: EMSL, a National scientific user facility at Pacific Northwest National Laboratory (PNNL); the Center for Nanoscale Materials at Argonne National Laboratory (ANL); and the National Energy Research Scientific Computing Center (NERSC). EMSL is sponsored by the Department of Energy's Office of Biological and Environmental Research located at PNNL. CNM and NERSC are supported by

the U.S. Department of Energy, Office of Science, under contracts DE-AC02-06CH11357 and DE-AC02-05CH11231, respectively.

Declarations of interest: none

References

[1] J. Sehested, Four challenges for nickel steam-reforming catalysts, Catal. Today 111 (2006) 103-110.

[2] A. Haryanto, S. Fernando, N. Murali, S. Adhikari, Current status of hydrogen production techniques by steam reforming of ethanol: A review, Energy Fuels 19 (2005) 2098-2106.

[3] J.R. Rostrup-Nielsen, J. Sehested, J.K. Nørskov, Hydrogen and synthesis gas by steam- and CO_2 reforming, Adv. Catal. 47 (2002) 65-139.

[4] J.K. Nørskov, T. Bligaard, A. Logadottir, S. Bahn, L. B. Hansen, M. Bollinger, H. Bengaard, B. Hammer, Z. Sljivancanin, M. Mavrikakis, Y. Xu, S. Dahl, C.J.H. Jacobsen, Universality in heterogeneous catalysis, J. Catal. 209 (2002) 275-278.

[5] A.N. Fatsikostas, X.E. Verykios, Reaction network of steam reforming of ethanol over Ni-based catalysts, J. Catal. 225 (2004) 439-452.

[6] R.M. Watwe, H.S. Bengaard, J.R. Rostrup-Nielsen, J.A. Dumesic, J.K. Nørskov, Theoretical studies of stability and reactivity of CH_x species on Ni(111), J. Catal. 189 (2000) 16-30.

[7] G. Jones, J.G. Jakobsen, S.S. Shim, J. Kleis, M.P. Andersson, J. Rossmeisl, F. Abild-Pedersen, T. Bligaard, S. Helveg, B. Hinnemann, J.R. Rostrup-Nielsen, I. Chorkendorff, J. Sehested, J.K. Nørskov, First principles calculations and experimental insight into methane steam reforming over transition metal catalysts, J. Catal. 259 (2008) 147-160.

[8] W. Wang, S.P. Wang, X.B. Ma, J.L. Gong, Recent advances in catalytic hydrogenation of carbon dioxide, Chem. Soc. Rev. 40 (2011) 3703-3727.

[9] J. Sehested, S. Dahl, J. Jacobsen, J.R. Rostrup-Nielsen, Methanation of CO over nickel: Mechanism and kinetics at high H_2/CO ratios, J. Phys. Chem. B 109 (2005) 2432-2438.

[10] I. Alstrup, On the kinetics of CO methanation on nickel surfaces, J. Catal. 151 (1995) 216-225.

[11] M.P. Andersson, E. Abild-Pedersen, I.N. Remediakis, T. Bligaard, G. Jones, J. Engbwk, O. Lytken, S. Horch, J.H. Nielsen, J. Sehested, J.R. Rostrup-Nielsen, J.K. Nørskov, I. Chorkendorff, Structure sensitivity of the methanation reaction: H_2-induced CO dissociation on nickel surfaces, J. Catal. 255 (2008) 6-19.

[12] J. Zhao, W.Q. Yu, C. Chen, H. Miao, H. Ma, J. Xu, Ni/NaX: A bifunctional efficient catalyst for selective hydrogenolysis of glycerol, Catal. Lett. 134 (2010) 184-189.

[13] A.G. Sergeev, J.D. Webb, J.F. Hartwig, A heterogeneous nickel catalyst for the hydrogenolysis of aryl ethers without arene hydrogenation, J. Am. Chem. Soc. 134 (2012) 20226-20229.

[14] J.H. Sinfelt, Catalytic hydrogenolysis on metals, Catal. Lett. 9 (1991) 159-172.

[15] S.Z. Tasker, E.A. Standley, T.F. Jamison, Recent advances in homogeneous nickel catalysis, Nature 509 (2014) 299-309.

[16] J. Montgomery, Nickel-catalyzed reductive cyclizations and couplings, Angew. Chem. Int. Ed. 43 (2004) 3890-3908.

[17] S.C. Singhal, Advances in solid oxide fuel cell technology, Solid State Ionics 135 (2000) 305-313.
[18] W. Wang, C. Su, Y.Z. Wu, R. Ran, Z.P. Shao, Progress in solid oxide fuel cells with nickel-based anodes operating on methane and related fuels, Chem. Rev. 113 (2013) 8104-8151.
[19] A.J. Jacobson, Materials for solid oxide fuel cells," Chem. Mater. 22 (2010) 660-674.
[20] D. Sutton, B. Kelleher, J.R.H. Ross, Review of literature on catalysts for biomass gasification, Fuel Process. Technol. 73 (2001) 155-173.
[21] D.C. Elliott, Catalytic hydrothermal gasification of biomass," Biofuels Bioprod. Biorefin. 2 (2008) 254-265.
[22] D.A. Bulushev, J.R.H. Ross, Catalysis for conversion of biomass to fuels via pyrolysis and gasification: A review, Catal. Today 171 (2011) 1-13.
[23] S.T. Oyama, T. Gott, H.Y. Zhao, Y.K. Lee, Transition metal phosphide hydroprocessing catalysts: A review, Catal. Today 143 (2009) 94-107.
[24] S.T. Oyama, Novel catalysts for advanced hydroprocessing: transition metal phosphides, J. Catal. 216 (2003) 343-352.
[25] C.S. Song, An overview of new approaches to deep desulfurization for ultra-clean gasoline, diesel fuel and jet fuel, Catal. Today 86 (2003) 211-263.
[26] K. Christma, O. Schober, G. Ertl, M. Neumann, Adsorption of hydrogen on nickel single-crystal surfaces, J. Chem. Phys. 60 (1974) 4528-4540.
[27] K. Christmann, R.J. Behm, G. Ertl, M.A. Vanhove, W.H. Weinberg, Chemisorption geometry of hydrogen on Ni(111) - Order and disorder, J. Chem. Phys. 70 (1979) 4168-4184.
[28] L. Hammer, H. Landskron, W. Nichtlpecher, A. Fricke, K. Heinz, K. Muller, Hydrogen-induced restructuring of close-packed metal-surfaces - H/Ni(111) and H/Fe(110), Phys. Rev. B 47 (1993) 15969-15972.
[29] H. Okuyama, T. Ueda, T. Aruga, M. Nishijima, Overtones of H vibrations at Ni(111): Formation of delocalized states, Phys. Rev. B 63 (2001) 233403.
[30] J.N. Russell, I. Chorkendorff, A.M. Lanzillotto, M.D. Alvey, J.T. Yates, Angular-distributions of H_2 thermal-desorption - Coverage dependence on Ni(111), J. Chem. Phys. 85 (1986) 6186-6191.
[31] K.J. Maynard, A.D. Johnson, S.P. Daley, S.T. Ceyer, A new mechanism for absorption - Collision-induced absorption, Faraday Discuss. 91 (1991) 437-449.
[32] A.D. Johnson, K.J. Maynard, S.P. Daley, Q.Y. Yang, S.T. Ceyer, Hydrogen embedded in Ni - Production by incident atomic-hydrogen and detection by high-resolution electron-energy loss, Phys. Rev. Lett. 67 (1991) 927-930.
[33] G.F.A. Vandewalle, H. Vankempen, P. Wyder, C.J. Flipse, Scanning tunneling microscopy and (scanning) tunneling spectroscopy on stepped Ni(111)/H, Surf. Sci. 181 (1987) 27-36.
[34] B. Bhatia, D.S. Sholl, Chemisorption and diffusion of hydrogen on surface and subsurface sites of flat and stepped nickel surfaces, J. Chem. Phys. 122 (2005) 204707.
[35] J. Greeley, M. Mavrikakis, A first-principles study of surface and subsurface H on and in Ni(111): diffusional properties and coverage-dependent behavior, Surf. Sci. 540 (2003) 215-229.

[36] P. Ferrin, S. Kandoi, A.U. Nilekar, M. Mavrikakis, M. Hydrogen adsorption, absorption and diffusion on and in transition metal surfaces: A DFT study, Surf. Sci. 606 (2012) 679-689.

[37] A.D. Johnson, S.P. Daley, A.L. Utz, S.T. Ceyer, The chemistry of bulk hydrogen - Reaction of hydrogen embedded in nickel with adsorbed CH_3, Science 257 (1992) 223-225.

[38] K.L. Haug, T. Burgi, T.R. Trautman, S.T. Ceyer, Distinctive reactivities of surface bound H and bulk H for the catalytic hydrogenation of acetylene, J. Am. Chem. Soc. 120 (1998) 8885-8886.

[39] S.P. Daley, A.L. Utz, T.R. Trautman, S.T. Ceyer, Ethylene hydrogenation on Ni(111) by bulk hydrogen, J. Am. Chem. Soc. 116 (1994) 6001-6002.

[40] S.T. Ceyer, The unique chemistry of hydrogen beneath the surface: Catalytic hydrogenation of hydrocarbons, Acc. Chem. Res. 34 (2001) 737-744.

[41] G.W. Peng, S.J. Sibener, G.C. Schatz, M. Mavrikakis, CO_2 hydrogenation to formic acid on Ni(110), Surf. Sci. 606 (2012) 1050-1055.

[42] J. Greeley, W.R. Krekelberg, M. Mavrikakis, Strain-induced formation of subsurface species in transition metals, Angew. Chem. Int. Ed. 43 (2004) 4296-4300.

[43] F.E. Celik, M. Mavrikakis, Stability of surface and subsurface hydrogen on and in Au/Ni near-surface alloys, Surf. Sci. 640 (2015) 190-197.

[44] G.W. Peng, S.J. Sibener, G.C. Schatz, S.T. Ceyer, Mavrikakis, M. CO_2 Hydrogenation to Formic Acid on Ni(111), J. Phys. Chem. C 116 (2012) 3001-3006.

[45] H.S. Bengaard, J.K. Nørskov, J. Sehested, B.S. Clausen, L.P. Nielsen, A.M. Molenbroek, J.R. Rostrup-Nielsen, Steam reforming and graphite formation on Ni catalysts, J. Catal. 209 (2002) 365-384.

[46] J. Gao, Y. Wang, Y. Ping, D. Hu, G. Xu, F. Gu, F. Su, A thermodynamic analysis of methanation reactions of carbon oxides for the production of synthetic natural gas, RSC Adv. 2 (2012) 2358-2368.

[47] A. Grossmann, W. Erley, H. Ibach, Adsorbate-induced surface stress and surface reconstruction - Oxygen, sulfur and carbon on Ni(111), Surf. Sci. 337 (1995) 183-189.

[48] C. Klink, I. Stensgaard, F. Besenbacher, E. Laegsgaard, An STM study of carbon-induced structures on Ni(111) - Evidence for a carbidic-phase clock reconstruction, Surf. Sci. 342 (1995) 250-260.

[49] D.E. Gardin, J.D. Batteas, M.A. Vanhove, G.A. Somorjai, Carbon, nitrogen, and sulfur on Ni(111) - Formation of complex structures and consequences for molecular decomposition," Surf. Sci. 296 (1993) 25-35.

[50] J. Mccarrol, T. Edmonds, R. Pitkethl, Interpretation of a complex low energy electron diffraction pattern - Carbonaceous and sulphur-containing structures on Ni(3), Nature 223 (1969) 1260-&.

[51] R. Backer, G. Horz, Scanning-tunneling-microscopy of carbon-induced and sulfur-induced modifications of Ni(111) and Ni(110) surfaces, Vacuum 46 (1995) 1101-1104.

[52] Y.A. Zhu, Y.C. Dai, D. Chen, W.K. Yuan, First-principles study of C chemisorption and diffusion on the surface and in the subsurfaces of Ni(111) during the growth of carbon nanofibers, Surf. Sci. 601 (2007) 1319-1325.

[53] T. Li, B. Bhatia, D.S. Sholl, First-principles study of C adsorption, O adsorption, and CO dissociation on flat and stepped Ni surfaces, J. Chem. Phys. 121 (2004) 10241-10249.

[54] S.G. Wang, X.Y. Liao, D.B. Cao, Y.W. Li, J.G. Wang, H.J. Jiao, Formation of carbon species on Ni(111): Structure and stability, J. Phys. Chem. C 111 (2007) 10894-10903.
[55] P.H. Hollowaya, J.B. Hudsona, Kinetics of the reaction of oxygen with clean nickel single crystal surfaces: II. Ni(111) surface, Surf. Sci. 43 (1974) 141-149.
[56] W. Altmann, K. Desinger, M. Donath, V. Dose, A. Goldmann, H. Scheidt, Dispersion of an empty adsorbate band - the P(2x2) oxygen overlayer on Ni(111), Surf. Sci. 151 (1985) L185-L190.
[57] P.M. Marcus, J.E. Demuth, D.W. Jepsen, Determination of the structure of ordered adsorbed layers by analysis of LEED spectra, Surf. Sci. 53 (1975) 501-522.
[58] M.A. Mendez, W. Oed, A. Fricke, L. Hammer, K. Heinz, K. Muller, Leed structure-analysis of p(√3 x √3)r30º-O/Ni(111)," Surf. Sci. 253 (1991) 99-106.
[59] D.T.V. Grimsby, Y.K. Wu, K.A.R. Mitchell, A Leed analysis for the Ni(111)-(2 X 2)-O surface-structure - Evidence for oxygen-induced relaxations of both vertical and lateral types in the close packed surface-layer of nickel, Surf. Sci. 232 (1990) 51-55.
[60] M. Pedio, L. Becker, B. Hillert, S. Daddato, J. Haase, Oxygen on Ni(111) - a Multiple-Scattering Analysis of the near-Edge X-Ray-Absorption Fine-Structure, Phys, Rev. B 41 (1990) 7462-7466.
[61] L.S. Caputi, S.L. Jiang, A. Amoddeo, R. Tucci, Oxygen-nickel bond length in Ni(111)-p(2x2)O determined by electron-energy-loss fine-structure spectroscopy, Phys. Rev. B 41 (1990) 8513-8515.
[62] L.S. Caputi, S.L. Jiang, R. Tucci, A. Amoddeo, L. Papagno, Oxygen-induced relaxation of Ni(111), Surf. Sci. 211 (1989) 120-124.
[63] T. Narusawa, W.M. Gibson, E. Tornqvist, Relaxation of Ni(111) surface by oxygen-adsorption, Phys. Rev. Lett. 47 (1981) 417-420.
[64] J.T. Stuckless, C.E. Wartnaby, N. AlSarraf, S.J.B. DixonWarren, M. Kovar, D.A. King, Oxygen chemisorption and oxide film growth on Ni{100}, {110}, and {111}: Sticking probabilities and microcalorimetric adsorption heats, J. Chem. Phys. 106 (1997) 2012-2030.
[65] J. Haase, B. Hillert, L. Becker, M. Pedio, A Sexafs study of the p(2 X 2)-O/Ni(111) system," Surf. Sci. 262 (1992) 8-14.
[66] H. Ibach, D. Bruchmann, Observation of surface phonons on Ni(111) by electron energy-loss spectroscopy, Phys. Rev. Lett. 44 (1980) 36-39.
[67] G.T. Tyuliev, K.L. Kostov, XPS/HREELS study of NiO films grown on Ni(111), Phys. Rev. B 60 (1999) 2900-2907.
[68] S. Hildebrandt, C. Hagendorf, T. Doege, C. Jeckstiess, R. Kulla, H. Neddermeyer, T. Uttich, Real time scanning tunneling microscopy study of the initial stages of oxidation of Ni(111) between 400 and 470 K, J.Vac. Sci. Technol. A 18 (2000) 1010-1015.
[69] G.W. Peng, L.R. Merte, J. Knudsen, R.T. Vang, E. Laegsgaard, F. Besenbacher, M. Mavrikakis, On the mechanism of low-temperature CO oxidation on Ni(111) and NiO(111) surfaces, J. Phys. Chem. C 114 (2010) 21579-21584.
[70] N.K. Das, T. Shoji, T. A density functional study of atomic oxygen and water molecule adsorption on Ni(111) and chromium-substituted Ni(111) surfaces, Appl. Surf. Sci. 258 (2011) 442-447.
[71] V. Maurice, N. Kitakatsu, M. Siegers, P. Marcus, Low-coverage sulfur induced reconstruction of Ni(111), Surf. Sci. 373 (1997) 307-317.

[72] L. Ruan, I. Stensgaard, F. Besenbacher, E. Laegsgaard, Observation of a missing-row structure on an Fcc(111) surface - the (5-Root-3x2)S phase on Ni(111) studied by scanning-tunneling-microscopy, Phys. Rev. Lett. 71 (1993) 2963-2966.

[73] W. Erley, H. Wagner, Sulfur poisoning of carbon-monoxide adsorption on Ni(111), J. Catal. 53 (1978) 287-294.

[74] T. Edmonds, J.J. McCarroll, R.C. Pitkethly, Surface structures formed during the interaction of sulphur compounds with the (111) face of nickel, J. Vac. Sci. Technol. 8 (1971) 68-74.

[75] J.E. Demuth, D.W. Jepsen, P.M. Marcus, Crystallographic dependence of chemisorption bonding for sulfur on (001), (110), and (111) nickel, Phys. Rev. Lett. 32 (1974) 1182-1185.

[76] J. Ludecke, A.R.H.F. Ettema, S.M. Driver, G. Scragg, M. Kerkar, D.P. Woodruff, B.C.C. Cowie, R.G. Jones, S. Bastow, The structure of sulphur adsorption phases on Ni(111) studied by X-ray standing wavefield absorption, Surf. Sci. 366 (1996) 260-274.

[77] Y.K. Wu, K.A.R. Mitchell, A refined Leed structural determination for the surface designated Ni (111)-(2x2)-S, Can. J. Chem. 67 (1989) 1975-1979.

[78] M. Zharnikov, M. Weinelt, P. Zebisch, M. Stichler, H.P. Steinruck, Holography of clean and sulfur-covered Ni(111) using multiple wave-number photoelectron diffraction patterns, Surf. Sci. 334 (1995) 114-134.

[79] Mullins, D. R.; Huntley, D. R.; Overbury, S. H. The Nature of the Sulfur Induced Surface Reconstruction on Ni(111), Surface Science 1995, 323, L287-L292.

[80] D.R. Warburton, P.L. Wincott, G. Thornton, F.M. Quinn, D. Norman, Incorporation of sulfur into the (111) surface of nickel, Surf. Sci. 211 (1989) 71-81.

[81] T. Fauster, H. Durr, D. Hartwig, Determination of the geometry of sulfur on nickel surfaces by low-energy ion-scattering, Surf. Sci. 178 (1996) 657-666.

[82] D.R. Alfonso, Computational studies of experimentally observed structures of sulfur on metal surfaces, J. Phys. Chem. C 115 (2011) 17077-17091.

[83] N.M. Galea, E.S. Kadantsev, T. Ziegler, Studying reduction in solid oxide fuel cell activity with density functional theory-effects of hydrogen sulfide adsorption on nickel anode surface, J. Phys. Chem. C 111 (2007) 14457-14468.

[84] E.J. Albenze, A. Shamsi, Density functional theory study of hydrogen sulfide dissociation on bi-metallic Ni-Mo catalysts, Surf. Sci. 600 (2006) 3202-3216.

[85] M. P. Kaminsky, N. Winograd, G.L. Geoffroy, M.A. Vannice, Direct sims observation of methylidyne, methylene, and methyl intermediates on a Ni(111) methanation catalyst, J. Am. Chem. Soc. 108 (1986) 1315-1316.

[86] S. Lehwald, H. Ibach, Decomposition of hydrocarbons on flat and stepped Ni(111) surfaces, Surf. Sci. 89 (1979) 425-445.

[87] M.B. Lee, Q.Y. Yang, S.T. Ceyer, Dynamics of the activated dissociative chemisorption of CH_4 and implication for the pressure gap in catalysis - a molecular-beam high-resolution electron-energy loss study, J. Chem. Phys. 87 (1987) 2724-2741.

[88] J.E. Demuth, H. Ibach, Identification of CH species on Ni(111) by high-resolution electron-energy loss spectroscopy, Surf. Sci. 78 (1978) L238-L244.

[89] Q.Y. Yang, K.J. Maynard, A.D. Johnson, S.T. Ceyer, The structure and chemistry of CH_3 and CH radicals adsorbed on Ni(111), J. Chem. Phys. 102 (1995) 7734-7749.

[90] J.E. Demuth, The interaction of acetylene with Ni(111), chemisorbed oxygen on Ni(111), and NiO(111); the formation of CH species on chemically modified Ni(111) surfaces, Surf. Sci. 69 (1977) 365-384.
[91] H. Burghgraef, A.P.J. Jansen, R.A. Vansanten, Methane activation and dehydrogenation on nickel and cobalt - a computational study, Surf. Sci. 324 (1995) 345-356.
[92] H. Yang, J.L. Whitten, Chemisorption of atomic-H and atomic-CH_x Fragments on Ni(111), Surf. Sci. 255 (1991) 193-207.
[93] S.G. Wang, D.B. Cao, Y.W. Li, J.G. Wang, H.J. Hao, CH_4 dissociation on Ni surfaces: Density functional theory study, Surf. Sci. 600 (2006) 3226-3234.
[94] A. Michaelides, P. Hu, Methyl chemisorption on Ni(111) and C-H-M multicentre bonding: a density functional theory study, Surf. Sci. 437 (1999) 362-376.
[95] G.A. Sargent, G.B. Freeman, J.L.R. Chao, Adsorption of CO on, and S poisoning of, a Perfect Ni(111) single-crystal and a Ni(111) crystal with small-angle boundaries, Surf. Sci. 100 (1980) 342-352.
[96] K. Christma, O. Schober, G. Ertl, Adsorption of CO on a Ni(111) Surface, J. Chem. Phys. 60 (1974) 4719-4724.
[97] H. Conrad, G. Ertl, J. Kuppers, E.E Latta, Adsorption of CO on clean and oxygen covered Ni(111) surfaces, Surf. Sci. 57 (1976) 475-484.
[98] J.C. Campuzano, R.G. Greenler, The adsorption sites of CO on Ni(111) as determined by infrared reflection-absorption spectroscopy, Surf. Sci. 83 (1979) 301.
[99] Z. Xu, L. Surnev, K.J. Uram, J.T. Yates, Interactions between chemisorbed CO and oxygen on Ni(111), Surf. Sci. 292 (1993) 235-247.
[100] W. Braun, H.P. Steinruck, G. Held, The surface geometries of the medium and high coverage carbon monoxide structures c(2 x 4)-(2CO) and p(√7 x √7-)R19º-(4CO) on Ni{111}, Surf. Sci. 575 (2005) 343-357.
[101] M.E. Davila, M.C. Asensio, D.P. Woodruff, K.M. Schindler, P. Hofmann, K.U. Weiss, R. Dippel, P. Gardner, V. Fritzsche, A.M. Bradshaw, J.C. Conesa, A.R. Gonzalezelipe, Structure determination of Ni(111)C(4x2)-CO and its implications for the interpretation of vibrational spectroscopic data, Surf. Sci. 311 (1994) 337-348.
[102] L.D. Mapledoram, M.P. Bessent, A. Wander, D.A. King, An automated tensor Leed analysis of the Ni(111)-C(4x2)-2CO structure, Chem. Phys. Lett. 228 (1994) 527-532.
[103] L. Becker, S. Aminpirooz, B. Hillert, M. Pedio, J. Haase, D.L. Adams, Threefold-coordinated hollow adsorption site for Ni(111)-C(4x2)-CO - a surface-extended x-ray-absorption fine-structure study, Phys. Rev. B 47 (1993) 9710-9714.
[104] W. Erley, H. Wagner, H. Ibach, Adsorption sites and long-range order - vibrational-spectra for CO on Ni(111), Surf. Sci. 80 (1979) 612-619.
[105] J.D. Beckerle, Q.Y. Yang, A.D. Johnson, S.T. Ceyer, The adsorption of CO and O_2 on Ni(111) at 8 K, Surf. Sci. 195 (1988) 77-93.
[106] L. Surnev, Z. Xu, J.T, Yates, Iras study of the adsorption of CO on Ni(111) - Interrelation between various bonding modes of chemisorbed CO, Surf. Sci. 201 (1988) 1-13.
[107] A. Beniya, N. Isomura, H. Hirata, Y. Watanabe, Low temperature adsorption and site-conversion process of CO on the Ni(111) surface, Surf. Sci. 606 (2012) 1830-1836.
[108] J.G. Chen, W. Erley, H. Ibach, A FT-Rairs investigation of the nature of the 3-fold bridge-CO species on Ni(111), Surf. Sci. 223 (1989) L891-L896.

[109] G. Held, J. Schuler, V. Sklarek, H.P. Steinruck, Determination of adsorption sites of pure and coadsorbed CO on Ni(111) by high resolution X-ray photoelectron spectroscopy, Surf. Sci. 398 (1998) 154-171.
[110] K. Kosmider, Theoretical study of CO and Pb adsorption on the Ni(111) and Ni_3Al(111) surfaces, Appl. Surf. Sci. 256 (2010) 4806-4812.
[111] A. Eichler, CO adsorption on Ni(111) - a density functional theory study, Surf. Sci. 526 (2003) 332-340.
[112] S. Stolbov, T.S. Rahman, First-principles study of some factors controlling the rate of ammonia decomposition on Ni and Pd surfaces, J. Chem. Phys. 123 (2005) 204716.
[113] J.C. Ganley, F.S. Thomas, E.G. Seebauer, R.I. Masel, A priori catalytic activity correlations: the difficult case of hydrogen production from ammonia, Catal. Lett. 96 (2004) 117-122.
[114] R.V. Hardeveld, A.V. Montfoort, The influence of crystallite size on the adsorption of molecular nitrogen on nickel, palladium and platinum: An infrared and electron-microscopic study, Surf. Sci. 4 (1966) 396-430.
[115] A. Quick, V.M. Browne, S.G. Fox, P. Hollins, Interactions of N_2 molecules adsorbed on smooth and roughened Ni(111) surfaces, Surf. Sci. 221 (1989) 48-60.
[116] J. Yoshinobu, R. Zenobi, J.Z. Xu, Z. Xu, J.T. Yates, N_2 chemisorption on Ni(111) - an infrared investigation under steady-state conditions, J. Chem. Phys. 95 (1991) 9393-9400.
[117] C.N.R. Rao, G.R. Rao, Nature of nitrogen adsorbed on transition-metal surfaces as revealed by electron-spectroscopy and cognate techniques," Surf. Sci. Rep. 13 (1991) 221-263.
[118] G.R. Rao, C.N.R. Rao, Adsorption of nitrogen on clean and modified single-crystal Ni surfaces, Appl. Surf. Sci. 45 (1990) 65-69.
[119] M.J. Breitschafter, E. Umbach, D. Menzel, Characterization of mixed N_2-layers on Ni(111) in the temperature-range 20-100 K, Surf. Sci. 178 (1986) 725-734.
[120] S. Masuda, R. Suzuki, M. Aoki, Local electron distribution of N_2 adsorbed on a Ni(111) surface probed by metastable impact electron spectroscopy, J. Chem. Phys. 113 (2000) 3864-3867.
[121] J.L. Gland, G.B. Fisher, G.E. Mitchell, Vibrational characterization of adsorbed NH on the Ni(111) Surface, Chem. Phys. Lett. 119 (1985) 89-92.
[122] T.E. Madey, J.E. Houston, The structure of NH_3 on Ni(111), J. Vac. Sci. Technol. 18 (1981) 476-480.
[123] C.W. Seabury, T.N. Rhodin, R.J. Purtell, R.P. Merrill, Chemisorption and reaction of NH_3 on Ni(111), Surf. Sci. 93 (1980) 117-126.
[124] F.P. Netzer, T.E. Madey, Interaction of NH_3 with oxygen-predosed Ni(111), Surf. Sci. 119 (1982) 422-432.
[125] G.B. Fisher, G.E. Mitchell, A vibrational study of ammonia chemisorbed on Ni(110) and Ni(111) - Whither goest the metal-nitrogen stretching mode on fcc (111) surfaces, J. Electron Spectrosc. Relat. Phenom. 29 (1983) 253-259.
[126] F. Bozso, J.M. Arias, C.P. Hanrahan, J.T. Yates, H. Metiu, R.M. Martin, A surface penning ionization study of NH_3 on Ni(111), Surf. Sci. 138 (1984) 488-504.
[127] M.J. Dresser, A.M. Lanzillotto, M.D. Alvey, J.T. Yates, Interaction between NH_3 and CO on the Ni(111) and (110) surfaces - a study by Esdiad, Surf. Sci. 191 (1987) 1-14.
[128] K.M. Schindler, V. Fritzsche, M.C. Asensio, P. Gardner, D.E. Ricken, A.W. Robinson, A.M. Bradshaw, D.P. Woodruff, J.C. Conesa, A.R. Gonzalezelipe, Structural

determination of a molecular adsorbate by photoelectron diffraction - Ammonia on Ni(111), Phys. Rev. B 46 (1992) 4836-4843.
[129] Z. Xu, L. Hanley, J.T. Yates, Layer interactions between dissimilar adsorbates - NH_3 layers on chemisorbed CO on Ni(111) - a reflection infrared Study, J. Chem. Phys. 96 (1992) 1621-1627.
[130] X.Z. Duan, J. Ji, G. Qian, C. Fan, Y. Zhu, X.G. Zhou, D. Chen, W.K. Yuan, Ammonia decomposition on Fe(110), Co(111) and Ni(111) surfaces: A density functional theory study, J. Mol. Catal. A Chem. 357 (2012) 81-86.
[131] B. Diawara, L. Joubert, D. Costa, P. Marcus, C. Adamo, Ammonia on Ni(111) surface studied by first principles: Bonding, multilayers structure and comparison with experimental IR and XPS data, Surf. Sci. 603 (2009) 3025-3034.
[132] A. Chattopadhyay, H. Yang, J.L. Whitten, Adsorption of ammonia on Ni(111), J. Phys. Chem. 94 (1990) 6379-6383.
[133] T. Kurten, M. Biczysko, T. Rajamaki, K. Laasonen, L. Halonen, Computational study of the adsorption energetics and vibrational wavenumbers of NH_3 adsorbed on the Ni(111) surface, J. Phys. Chem. B 109 (2005) 8954-8960.
[134] E. Salli, V. Hanninen, L. Halonen, Variationally calculated vibrational energy levels of ammonia adsorbed on a Ni(111) surface, J. Phys. Chem. C 114 (2010) 4550-4556.
[135] M.J. Breitschafter, E. Umbach, D. Menzel, An electron spectroscopic investigation of the adsorption of NO on Ni(111), Surf. Sci. 109 (1981) 493-511.
[136] F.P. Netzer, T.E. Madey, The adsorption of NO on Ni(111) - an Esdiad-Leed study, Surf. Sci. 110 (1981) 251-260.
[137] W. Erley, Infrared-spectroscopy of NO adsorbed on Ni(111) at 85 K, Surf. Sci. 205 (1988) L771-L776.
[138] H. Conrad, G. Ertl, J. Kuppers, E.E. Latta, Interaction of NO with a Ni(111) surface, Surf. Sci. 50 (1975) 296-310.
[139] F. Bozso, J. Arias, C.P. Hanrahan, J.T. Yates, R.M. Martin, H. Metiu, Study of adsorption and decomposition of NO on clean and oxygen-covered Ni(111) by metastable quenching spectroscopy, Surf. Sci. 141 (1984) 591-603.
[140] J.G. Chen, W. Erley, H. Ibach, A Rairs investigation of the interaction between the coadsorbed NO and oxygen on Ni(111) - Observation of a substantial N-O bond strengthening, Surf. Sci. 224 (1989) 215-234.
[141] J.G. Chen, W. Erley, H. Ibach, A Rairs observation of the local interaction between coadsorbed NO and CO on Ni(111), Surf. Sci. 227 (1990) 79-89.
[142] T.T. Magkoev, M.B. Song, K. Fukutani, Y. Murata, Interaction of ultraviolet photons with NO/Ni(111), Surf. Sci. 363 (1996) 281-288.
[143] W. Erley, B.N.J. Persson, Vibrational lineshapes for NO on Ni(111), Surf. Sci. 218 (1989) 494-506.
[144] T.T. Magkoev, M.B. Song, K. Fukutani, Y. Murata, Rairs observation of photoinduced dissociation of NO on Ni(111), Surf. Sci. 330 (1995) L669-L672.
[145] R. Lindsay, A. Theobald, T. Giessel, O. Schaff, A.M. Bradshaw, N.A. Booth, D.P. Woodruff, The structure of NO on Ni(111) at low coverage, Surf. Sci. 405 (1998) L566-L572.
[146] N. Materer, A. Barbieri, D. Gardin, U. Starke, J.D. Batteas, M.A.Vanhove, G.A. Somorjai, Hollow-site molecular adsorption for NO on Pt(111) and Ni(111) - Invalidating vibrational site assignment rules, Phys. Rev. B 48 (1993) 2859-2861.

[147] N. Materer, A. Barbieri, D. Gardin, U. Starke, J.D. Batteas, M.A. Vanhove, G.A. Somorjai, Dynamical Leed analyses of the Pt(111)-p(2x2)-NO and the Ni(111)-c(4x2)-2NO structures - Substrate relaxation and unexpected hollow-site adsorption, Surf. Sci. 303 (1994) 319-332.

[148] M.C. Asensio, D.P. Woodruff, A.W. Robinson, K.M. Schindler, P. Gardner, D. Ricken, A.M. Bradshaw, J.C. Conesa, A.R. Gonzalezelipe, Single local site structure for vibrationally distinct adsorption states - NO on Ni(111), Chem. Phys. Lett. 192 (1992) 259-264.

[149] H.P. Steinruck, C. Schneider, P.A. Heimann, T. Pache, E. Umbach, D. Menzel, Electronic-Structure and orientation of NO on Ni(111) studied by ARUPS using synchrotron radiation, Surf. Sci. 208 (1989) 136-154.

[150] M.C. Asensio, D.P. Woodruff, A.W. Robinson, K.M. Schindler, P. Gardner, D. Ricken, A.M. Bradshaw, J.C. Conesa, A.R. Gonzalezelipe, Local site identification for NO on Ni(111) in vibrationally distinct adsorption states, J. Vac. Sci. Technol. A 10 (1992) 2445-2450.

[151] S. Aminpirooz, A. Schmalz, L. Becker, J. Haase, J. Threefold-coordinated hollow adsorption site for c(4x2)-NO/Ni(111) - a surface-extended X-ray-absorption fine-structure study," Phys. Rev. B 45 (1992) 6337-6340.

[152] S.Y. Wu, J.J. Ho, The interaction of NO_x on Ni(111) surface investigated with quantum-chemical calculations, Phys. Chem. Chem. Phys. 12 (2010) 13707-13714.

[153] M. Mavrikakis, J. Rempel, J. Greeley, L.B. Hansen, J.K. Nørskov, Atomic and molecular adsorption on Rh(111), J. Chem. Phys. 117 (2002) 6737-6744.

[154] W.P. Krekelberg, J. Greeley, M. Mavrikakis, Atomic and molecular adsorption on Ir(111), J. Phys. Chem. B 108 (2004) 987-994.

[155] D.C. Ford, Y. Xu, M. Mavrikakis, Atomic and molecular adsorption on Pt(111), Surf. Sci. 587, (2005) 159-174.

[156] J.A. Herron, S. Tonelli, M. Mavrikakis, Atomic and molecular adsorption on Pd(111), Surf. Sci. 606 (2012) 1670-1679.

[157] J.A. Herron, S. Tonelli, M. Mavrikakis, Atomic and molecular adsorption on Ru(0001), Surf. Sci. 614 (2013) 64-74.

[158] K. Hahn, M. Mavrikakis, Atomic and Molecular Adsorption on Re(0001), Top. Catal. 57 (2014) 54-68.

[159] Y. Santiago-Rodriguez, J.A. Herron, M.C. Curet-Arana, M. Mavrikakis, Atomic and molecular adsorption on Au(111), Surf. Sci. 627 (2014) 57-69.

[160] L. Xu, D. Kirvassilis, Y. Bai, M. Mavrikakis, Atomic and molecular adsorption on Fe(110), Surf. Sci. 667 (2018) 54-65.

[161] B.W.J. Chen, D. Kirvassilis, Y. Bai, M. Mavrikakis, Atomic and molecular adsorption on Ag(111), J. Phys. Chem. C (2018). DOI: 10.1021/acs.jpcc.7b11629

[162] L. Xu, J. Lin, Y. Bai, M. Mavrikakis, Atomic and molecular adsorption on Cu(111), Top. Catal. (2018). DOI: 10.1007/s11244-018-0943-0

[163] J.S. Hummelshoj, F. Abild-Pedersen, F. Studt, T. Bligaard, J.K. Nørskov, CatApp: A web application for surface chemistry and heterogeneous catalysis, Angew. Chem. Int. Ed. 51 (2012) 272-274.

[164] B. Hammer, L.B. Hansen, J.K. Nørskov, Improved adsorption energetics within density-functional theory using revised Perdew-Burke-Ernzerhof functionals," Phys. Rev. B 59 (1999) 7413-7421.

[165] J. Greeley, J.K. Nørskov, M. Mavrikakis, Electronic structure and catalysis on metal surfaces, Annu. Rev. Phys. Chem. 53 (2002) 319-348.
[166] J. Neugebauer, M. Scheffler, Adsorbate-substrate and adsorbate-adsorbate interactions of Na and K Adlayers on Al(111), Phys. Rev. B 46 (1992) 16067-16080.
[167] L. Bengtsson, Dipole correction for surface supercell calculations, Phys. Rev. B 59 (1999) 12301-12304.
[168] D.J. Chadi, M.I. Cohen, Special points in the brillouin zone, Phys. Rev. B 8 (1973) 5747-5753.
[169] D. Vanderbilt, Soft self-consistent pseudopotentials in a generalized eigenvalue formalism, Phys. Rev. B 41 (1990) 7892-7895.
[170] J.P. Perdew, Y. Wang, Accurate and simple analytic representation of the electron-gas correlation-energy, Phys. Rev. B 45 (1992) 13244-13249.
[171] J.A. White, D.M. Bird, Implementation of gradient-corrected exchange-correlation potentials in car-parrinello total-energy calculations, Phys. Rev. B 50 (1994) 4954-4957.
[172] G. Kresse, J. Furthmuller, Efficiency of ab-initio total energy calculations for metals and semiconductors using a plane-wave basis set, Comput. Mater. Sci. 6 (1996) 15-50.
[173] CRC Handbook of Chemistry and Physics; 76 th ed.; CRC Press (1996).
[174] M.B. Stearns, 1.1.2.4 Spontaneous magnetization, magnetic moments and high-field susceptibility: Datasheet from Landolt-Börnstein - Group III Condensed Matter · Volume 19A: "3d, 4d and 5d Elements, Alloys and Compounds" in SpringerMaterials (https://dx.doi.org/10.1007/10311893_7) (1986).
[175] R.D.I. Johnson, NIST Computational Chemistry Comparison and Benchmark Database, NIST Standard Reference, Database Number 101 (2004).
[176] J. Lapujoulade, K.S. Neil, Chemisorption of hydrogen on the (111) plane of nickel, J. Chem. Phys. 57 (1972) 3535.
[177] A. Papagno, N. Pacile, C. Giallombardo, A. Cupolillo, L. Papagno, HREEL study of c(5√3 x 9)rect-N structure on Ni(111) surface, J. Electron Spectrosc. Relat. Phenom. 148 (2005) 164-169.
[178] H. Yang, J.L. Whitten, Dissociative adsorption of H_2 on Ni(111), J. Chem. Phys. 98 (1993) 5039-5049.
[179] G. Kresse, J. Hafner, First-principles study of the adsorption of atomic H on Ni(111), (100) and (110), Surf. Sci. 459 (2000) 287-302.
[180] Y. Shizuku, S. Yamamoto, Y. Fukai, Phase diagram of the Ni-H system at high hydrogen pressures, J. Alloys Compd. 336 (2002) 159-162.
[181] Y. Fukai, S. Yamatomo, S. Harada, M. Kanazawa, The phase diagram of the Ni-H system revisited, J. Alloys Compd. 372 (2004) L4-L5.
[182] G. Gross, K.H. Rieder, He-diffraction investigations of the (2 x 2)-phases of oxygen and hydrogen on Ni(111), Surf. Sci. 241 (1991) 33-38.
[183] G.X. Cao, E. Nabighian, X.D. Zhu, Diffusion of hydrogen on Ni(111) over a wide range of temperature: Exploring quantum diffusion on metals, Phys. Rev. Lett. 79 (1997) 3696-3699.
[184] F. Besenbacher, J.K. Nørskov, Oxygen-chemisorption on metal-surfaces - general trends for Cu, Ni and Ag, Prog. Surf. Sci. 44 (1993) 5-66.
[185] S.J. Carey, W. Zhao, A. Frehner, C.T. Campbell, Energetics of adsorbed methyl and methyl iodide on Ni(111) by calorimetry: Comparison to Pt(111) and implications for catalysis, ACS Catal. 7 (2017) 1286-1294.

[186] L.D. Mapledoram, A. Wander, D.A. King, Breakdown of adsorbate site assignment from vibrational frequencies - NO on Ni(111) revisited by tensor Leed, Chem. Phys. Lett. 208 (1993) 409-413.
[187] L.S. Caputi, G. Chiarello, S. Molinaro, R.G. Agostino, A. Amoddeo, E. Colavita, Hreels investigation of the coadsorption of CO and NO on Ni(111) at room-temperature, J. Electron Spectrosc. Relat. Phenom. 64-5 (1993) 145-149.
[188] J. Shan, A.W. Kleyn, L.B.F. Juurlink, Identification of hydroxyl on Ni(111), Chemphyschem 10 (2009) 270-275.
[189] J.B. Miller, H.R. Siddiqui, S.M. Gates, J.N. Russell, J.T. Yates, J.C. Tully, M.J. Cardillo, Extraction of kinetic-parameters in temperature programmed desorption - a comparison of methods, J. Chem. Phys. 87 (1987) 6725-6732.
[190] T.S. Lin, H.J. Lu, R. Gomer, Diffusion of CO on Ni(111) and Ni(115), Surf. Sci. 234 (1990) 251-261.
[191] M.J. Harrison, D.P. Woodruff, J. Robinson, Density functional theory investigation of CN on Cu(111), Ni(111) and Ni(100)," Surf. Sci. 600 (2006) 340-347.
[192] H. Yang, T.C. Caves, J.L. Whitten, Ab-Initio studies of CN adsorbed on Ni(111), J. Chem. Phys. 103 (1995) 8756-8763.
[193] H. Yang, Ab initio embedding studies of chemisorption on metal surfaces - interaction of small C-N containing molecules with Ni(111), J. Mol. Catal. A Chem. 119 (1997) 425-436.
[194] M.E. Kordesch, T. Lindner, J. Somers, W. Stenzel, H. Conrad, A.M. Bradshaw, G.P. Williams, The surface chemistry of the CN Group - geometry and bonding, Spectrochim. Acta A 43 (1987) 1561-1566.
[195] C. Oliva, C. van den Berg, J.W.H. Niemantsverdriet, D. Curulla-Ferre, A density functional theory study of HCN hydrogenation to methylamine on Ni(111)," J. Catal. 245 (2007) 436-445.
[196] P.L. Hagans, I. Chorkendorff, J.T. Yates, Scanning kinetic spectroscopy and temperature-programmed desorption studies of the adsorption and decomposition of HCN on the Ni(111) surface, J. Phys. Chem. 92 (1988) 471-476.
[197] M. Ojeda, R. Nabar, A.U. Nilekar, A. Ishikawa, M. Mavrikakis, E. Iglesia, CO activation pathways and the mechanism of Fischer-Tropsch synthesis, J. Catal. 272 (2010) 287-297.
[198] M.P. Andersson, F. Abild-Pedersen, I.N. Remediakis, T. Bligaard, G. Jones, J. Engbæk, O. Lytken, S. Horch, J.H. Nielsen, J. Sehested, J.R. Rostrup-Nielsen, J.K. Nørskov, I. Chorkendorff, Structure sensitivity of the methanation reaction: H_2-Induced CO dissociation on nickel surfaces, J. Catal. 255 (2008) 6-19.
[199] L.C. Grabow, M. Mavrikakis, Mechanism of methanol synthesis on Cu through CO_2 and CO hydrogenation, ACS Catal. 1 (2011) 365-384.
[200] C.A. Farberow, J.A. Dumesic, M. Mavrikakis, Density functional theory calculations and analysis of reaction pathways for reduction of nitric oxide by hydrogen on Pt(111)," ACS Catal. 4 (2014) 3307-3319.
[201] D.D. Hibbitts, R. Jimenez, M. Yoshimura, B. Weiss, E. Iglesia, Catalytic NO activation and NO-H_2 reaction pathways, J. Catal. 319 (2014) 95-109.
[202] J.L.C. Fajin, M.N.D.S. Cordeiro, J.R.B. Gomes, The role of preadsorbed atomic hydrogen in the NO dissociation on a zigzag stepped gold surface: A DFT study, J. Phys. Chem. C 113 (2009) 8864-8877.

[203] L.Y. Huai, C.Z. He, H. Wang, H. Wen, W.C. Yi, J.Y. Liu, NO dissociation and reduction by H_2 on Pd(111): A first-principles study, J. Catal. 322 (2015) 73-83.
[204] Y. Bai, M. Mavrikakis, Mechanistic study of nitric oxide reduction by hydrogen on Pt(100) (I): A DFT analysis of the reaction network, J. Phys. Chem. B 122 (2018) 432-443.
[205] W. Zhao, S.J. Carey, Z. Mao, C. T. Campbell, Adsorbed hydroxyl and water on Ni(111): Heats of formation by calorimetry, ACS Catal. 8 (2018) 1485-1498.
[206] S.X. Liu, T. Ishimoto, M. Koyama, First-principles study of oxygen coverage effect on hydrogen oxidation on Ni(111) surface, Appl. Surf. Sci. 333 (2015) 86-91.
[207] M. Pozzo, G. Carlini, R. Rosei, D. Alfe, Comparative study of water dissociation on Rh(111) and Ni(111) studied with first principles calculations, J. Chem. Phys. 126 (2007) 164706.
[208] H. Seenivasan, A.K. Tiwari, Water dissociation on Ni(100) and Ni(111): Effect of surface temperature on reactivity, J. Chem. Phys. 139 (2013) 174707.
[209] D.W. Blaylock, Y.A. Zhu, W.H. Green, Computational investigation of the thermochemistry and kinetics of steam methane reforming over a multi-faceted nickel catalyst, Top. Catal. 54 (2011) 828-844.
[210] A.D. Karmazyn, V. Fiorin, S.J. Jenkins, D.A. King, First-principles theory and microcalorimetry of CO adsorption on the {211} Surfaces of Pt and Ni, Surf. Sci. 538 (2003) 171-183.
[211] Q. Ge, S.J. Jenkins, D.A. King, Localisation of adsorbate-induced demagnetisation: CO chemisorbed on Ni{110}, Chem. Phys. Lett. 327 (2000) 125-130.
[212] S.J. Jenkins, Q. Ge, D.A. King, Covalent origin of adsorbate-induced demagnetization at ferromagnetic surfaces, Phys. Rev. B 64 (2001) 012413.
[213] S. Yamagishi, S.J. Jenkins, D.A. King, Symmetry and site selectivity in molecular chemisorption: Benzene on Ni{111}, J. Chem. Phys. 114 (2001) 5765-5773.
[214] F. Mittendorfer, J. Hafner, Density-functional study of the adsorption of benzene on the (1 1 1), (1 0 0) and (1 1 0) surfaces of nickel, Surf. Sci. 472 (2001) 133-153.

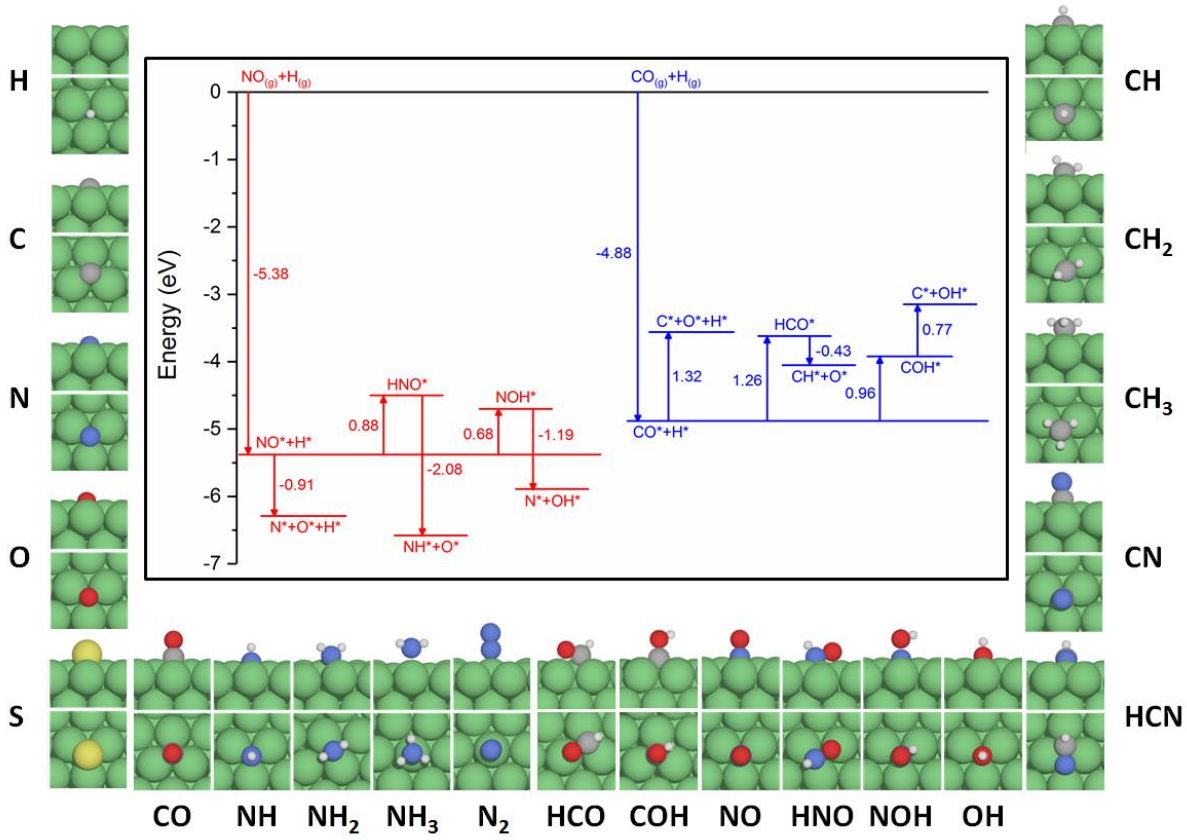

Graphical abstract